
Article:
Sassani, M., Alix, J., McDermott, C. et al. (6 more authors) (2020) Magnetic resonance spectroscopy reveals mitochondrial dysfunction in amyotrophic lateral sclerosis. Brain, 143 (12). pp. 3603-3618. ISSN 0006-8950

https://doi.org/10.1093/brain/awaa340

OXFORD UNIVERSITY PRESS | Brain

Magnetic resonance spectroscopy reveals mitochondrial dysfunction in amyotrophic lateral sclerosis

Journal:	*Brain*
Manuscript ID	BRAIN-2020-00812.R1
Manuscript Type:	Original Article
Date Submitted by the Author:	n/a
Complete List of Authors:	Sassani, Matilde; The University of Sheffield, Sheffield Institute for Translational Neuroscience Alix, James; The University of Sheffield, Sheffield Institute for Translational Neuroscience McDermott, Christopher; The University of Sheffield, Sheffield Institute for Translational Neuroscience Baster, Kathleen; The University of Sheffield, Statistical Services Unit Hoggard, Nigel; The University of Sheffield, Academic Unit of Radiology Wild, Jim; The University of Sheffield, Academic Unit of Radiology Mortiboys, Heather; The University of Sheffield, Sheffield Institute for Translational Neuroscience Shaw, Pamela; The University of Sheffield, Sheffield Institute for Translational Neuroscience Wilkinson, Iain; The University of Sheffield, Academic Unit of Radiology Jenkins, Thomas; The University of Sheffield, Sheffield Institute for Translational Neuroscience
Subject category:	Neuromuscular diseases
To search keyword list, use whole or part words followed by an *:	Amyotrophic lateral sclerosis < NEURODEGENERATION: CELLULAR AND MOLECULAR, Neuromuscular disease: imaging < NEUROMUSCULAR DISEASES, Neurodegeneration: biomarkers < NEURODEGENERATION: CELLULAR AND MOLECULAR, Denervation < NEUROMUSCULAR DISEASES, Imaging methodology < SYSTEMS/DEVELOPMENT/PHYSIOLOGY

Magnetic resonance spectroscopy reveals mitochondrial dysfunction in amyotrophic lateral sclerosis

[1]Sassani M*, [1]Alix JJ, [1]McDermott CJ, [2]Baster K, [3]Hoggard N, [3]Wild JM, [1]Mortiboys HJ, [1]Shaw PJ, [3]Wilkinson ID, [1]Jenkins TM.

[1]Sheffield Institute for Translational Neuroscience (SITraN), University of Sheffield, Sheffield, United Kingdom; [2]Statistical Service Unit, University of Sheffield, Sheffield, United Kingdom; [3]Academic Unit of Radiology, University of Sheffield, Sheffield, United Kingdom

Short title: Bioenergetics in ALS

*Corresponding author:
Dr Matilde Sassani
msassani1@sheffield.ac.uk
Sheffield Institute for Translational Neuroscience
University of Sheffield
385a Glossop Road
Sheffield
S10 2HQ
United Kingdom
T: +44 (0)114 222 2230

Abstract

Mitochondrial dysfunction is postulated to be central to amyotrophic lateral sclerosis pathophysiology. Evidence comes primarily from disease models and conclusive data to support bioenergetic dysfunction *in vivo* in patients is currently lacking. This study is the first to assess mitochondrial dysfunction in brain and muscle in people living with amyotrophic lateral sclerosis using phosphorus-31 magnetic resonance spectroscopy, the modality of choice to assess energy metabolism *in vivo*. We recruited twenty patients and 10 healthy age and gender-matched controls in this cross-sectional clinico-radiological study. Phosphorus-31 magnetic resonance spectroscopy was acquired from cerebral motor regions and from tibialis anterior during rest and exercise. Bioenergetic parameter estimates were derived including: adenosine triphosphate, phosphocreatine, inorganic phosphate, adenosine diphosphate, Gibbs free energy of adenosine triphosphate hydrolysis, phosphomonoesters, phosphodiesters, pH, free magnesium concentration, and muscle dynamic recovery constants. Linear regression was used to test for associations between brain data and clinical parameters (revised amyotrophic functional rating scale, slow vital capacity, and upper motor neuron score) and between muscle data and clinico-neurophysiological measures (motor unit number and size indices, force of contraction, and speed of walking).

Evidence for primary dysfunction of mitochondrial oxidative phosphorylation was detected in brainstem where Gibbs free energy of adenosine triphosphate hydrolysis and phosphocreatine were reduced. Alterations were also detected in skeletal muscle in patients where resting inorganic phosphate, pH, and phosphomonoesters were increased, whereas resting Gibbs free energy of adenosine triphosphate hydrolysis, magnesium, and dynamic phosphocreatine to inorganic phosphate recovery were decreased. Phosphocreatine in brainstem correlated with respiratory dysfunction and disability; in muscle, energy metabolites correlated with motor unit number index, muscle power, and speed of walking. This study provides *in vivo* evidence for

bioenergetic dysfunction in amyotrophic lateral sclerosis in brain and skeletal muscle, which appears clinically and electrophysiologically relevant. Phosphorus-31 magnetic resonance spectroscopy represents a promising technique to assess the pathophysiology of mitochondrial function *in vivo* in amyotrophic lateral sclerosis and a potential tool for future clinical trials targeting bioenergetic dysfunction.

Keywords

Amyotrophic lateral sclerosis, Neuromuscular disease: imaging, Neurodegeneration: biomarkers, Denervation, Imaging methodology.

Abbreviations

ADP=adenosine diphosphate, ALS=amyotrophic lateral sclerosis, CI=95% confidence interval, ΔG_{ATP}=Gibbs free energy of ATP hydrolysis, ^{31}P-MRS=phosphorus-31 magnetic resonance spectroscopy.

Introduction

Mitochondrial dysfunction is considered a key mechanism accompanying the relentless neurodegeneration seen in amyotrophic lateral sclerosis (ALS) (Dupuis *et al.*, 2011; Smith *et al.*, 2017; Vandoorne *et al.*, 2018), a devastating condition characterised by aggressive upper and lower motor neuron loss, resulting in progressive paralysis and death. Aetiology and pathophysiology remain incompletely understood, hampering development of effective treatments. Whilst defined genetic mutations explain approximately 10% of cases (Rosen *et al.*, 1993; Sreedharan *et al.*, 2008; Kwiatkowski *et al.*, 2009; DeJesus-Hernandez *et al.*, 2011; Renton *et al.*, 2011; Chiò *et al.*, 2012), sporadic ALS predominates and is considered to reflect multifactorial interplay of genetic and exogenous factors, resulting in a complex cascade of aberrant cellular processes and neurodegeneration (Shaw, 2005; Al-Chalabi and Hardiman, 2013; Al-Chalabi *et al.*, 2014; Chiò *et al.*, 2018).

Sporadic ALS is characterised by protein aggregates which may be directly and indirectly toxic to mitochondria (Smith *et al.*, 2017). Neurofilament aggregates within axons and hyper-phosphorylated ubiquitinated TDP-43 inclusions mislocalised within cell bodies are the cytopathological hallmarks of all sporadic and most familial cases (Neumann *et al.*, 2006). Misfolded TDP-43 may localise to mitochondria and is hypothesised to affect mitochondrial quality control, mitochondrial fission and fusion, mitochondrial axonal transport (Gao *et al.*, 2019), and to inhibit assembly of electron transport chain complex I by directly interfering with expression of ND3 and ND6 subunits (Wang *et al.*, 2016).

Stronger evidence for direct mitochondrial bioenergetic dysfunction has emerged from genetic disease models. In *C9orf72*-related ALS, dipeptide repeat proteins $(GR)_{80}$ bind mitochondrial ATP synthase (Choi *et al.*, 2019), increasing production of reactive oxygen species, and inducing DNA damage; mutant *C9orf72* fibroblasts demonstrate altered mitochondrial oxygen consumption and membrane potential (Onesto *et al.*, 2016). Mutant FUS can also directly bind

ATP synthase (Deng *et al.*, 2018) and cause toxicity indirectly through effects on mitochondrial gene translation (Nakaya and Maragkakis, 2018) and on mitochondrial-endoplasmic reticulum interactions (Stoica *et al.*, 2016). In the SOD1-G93A transgenic mouse, SOD1 aggregates alter oxidative phosphorylation even in the pre-symptomatic stage (Kirkinezos *et al.*, 2005), possibly through interactions with B-cell lymphoma two and voltage-dependent anion channels (Tan *et al.*, 2014). SOD1-induced impairment of electron transport chain in spinal cord and muscle results in altered energy metabolism increasing oxidative stress (Mattiazzi *et al.*, 2002; Mahoney *et al.*, 2006; Dobrowolny *et al.*, 2018), aberrant mitochondrial dynamics, and calcium handling (Damiano *et al.*, 2006; Zhou *et al.*, 2010; Luo *et al.*, 2013; Song *et al.*, 2013).

ALS can also develop through mutations in mitochondrial homeostatic genes including *VAPB*, *CHCHD10*, and *VCP*. VAPB is found at contact sites between mitochondria and endoplasmic reticulum and mutations cause intracellular calcium mishandling and aberrant mitochondrial axonal transport (De Vos *et al.*, 2012; Morotz *et al.*, 2012). CHCHD10 is located in the mitochondrial intermembrane space and is considered necessary for optimal electron transport chain function (Genin *et al.*, 2016; Burstein *et al.*, 2018; Lehmer *et al.*, 2018; Straub *et al.*, 2018). Lastly, mutations in *VCP* cause mitochondrial uncoupling (Bartolome *et al.*, 2013; Nalbandian *et al.*, 2015; Hall *et al.*, 2017; Ludtmann *et al.*, 2017). These studies collectively represent a body of evidence to support mitochondrial dysfunction as a common mechanism across ALS variants and suggest that bioenergetic dysfunction may affect both peripheral tissues and the CNS.

To date, conclusive data to support bioenergetic dysfunction in people living with ALS are lacking. No previous published studies have employed cranial phosphorus-31 magnetic resonance spectroscopy (^{31}P-MRS), the modality of choice to assess mitochondrial function *in vivo* in humans. ^{31}P-MRS has been applied to skeletal muscle in ALS, but previous results were discordant and limited by very small sample sizes (Zochodne *et al.*, 1988; Sharma *et al.*, 1995;

Kent-Braun and Miller, 2000; Grehl *et al.*, 2007; Ryan *et al.*, 2014). *Post mortem* studies in CNS mitochondria yielded conflicting results with some identifying electron transport chain inhibition in spinal cord (Fujita *et al.*, 1996; Borthwick *et al.*, 1999; Wiedemann *et al.*, 2002) and others changes only in motor cortex in SOD1 patients, but not in sporadic cases (Bowling *et al.*, 1993; Browne *et al.*, 1998). Histopathological studies of muscle demonstrate modest alterations of electron transport chain complex activity of unknown clinical significance (Wiedemann *et al.*, 1998; Vielhaber *et al.*, 1999; Krasnianski *et al.*, 2005; Echaniz-Laguna *et al.*, 2006; Soraru *et al.*, 2007; Crugnola *et al.*, 2010).

^{31}P-MRS allows quantification of ATP, phosphocreatine, inorganic phosphate, and membrane phospholipid precursors (phosphomonoesters) and catabolites (phosphodiesters), in brain and muscle, at rest and during exercise. More detailed characterisation of bioenergetic status is possible through calculation of intracellular pH (Rata *et al.*, 2014; Cichocka *et al.*, 2015), free magnesium (Iotti *et al.*, 1996, 2000; Iotti and Malucelli, 2008), and adenosine diphosphate (ADP) (Iotti *et al.*, 2005). In addition, the Gibbs free energy of ATP hydrolysis (ΔG_{ATP}) is quantifiable (Veech *et al.*, 1979; Iotti *et al.*, 2005), a thermodynamic parameter that quantifies useful energy released by ATP hydrolysis, calculated from ATP, inorganic phosphate, and ADP, and dependent on phosphocreatine concentration, reflecting whether cellular energy demand is met by mitochondrial ATP production (Nicholls, 2013; Kemp *et al.*, 2015).

Whilst cranial ^{31}P-MRS has been applied to identify disease-specific bioenergetic changes in anatomically relevant regions in Alzheimer's, Parkinson's, and Huntington's diseases (Hoang *et al.*, 1998; Hu *et al.*, 2000; Hattingen *et al.*, 2009; Weiduschat *et al.*, 2015; Rijpma *et al.*, 2018), this is the first study in ALS. The study aims are to characterise the bioenergetic metabolic profile *in vivo* in ALS, both in brain and skeletal muscle, and to determine whether any bioenergetic alterations are of clinical and neurophysiological relevance. We hypothesised that dysfunctional bioenergetic homeostasis will be reflected in alterations in inorganic

phosphate, phosphocreatine, and ADP resulting in abnormal ΔG_{ATP} measurements in patients compared to controls, and associate with disability, clinical weakness, and loss motor unit loss. ΔG_{ATP} may be a particularly important parameter to consider in ALS, as inability of cellular ATP synthesis to meet energy demand may be dysfunctional due to mitochondrial uncoupling or electron transport chain inhibition (Smith *et al.*, 2017), prior to any reduction in ATP becoming detectable.

Materials and methods

Research participants

Twenty patients and 10 age and gender-matched neurologically normal controls participated in this cross-sectional clinico-radiological study. Patients were recruited from Sheffield Teaching Hospitals NHS Foundation Trust tertiary referral neuromuscular clinics between November 2017 and August 2019. Patient inclusion criteria were a diagnosis of clinically possible, probable, or definite ALS, according to revised El-Escorial criteria (Brooks *et al.*, 2000). Exclusion criteria for all participants were: evidence of respiratory failure impairing ability to lie flat, cognitive problems impairing capacity for informed consent, pacemakers or other non-magnetic resonance compatible device, pregnancy, and current or previous additional neurological disease. The local research ethics committee approved the study (Yorkshire and the Humber REC 13/YH/0273) in accordance with the declaration of Helsinki. Written informed consent was obtained from all participants.

Clinical and neurophysiological data

The following data were acquired from all participants on the day of the scan: age, gender, weight, 10-metre walk test, and medical history of diabetes mellitus or pre-diabetic state. In patients, disease duration, revised ALS functional rating scale (Cedarbaum *et al.*, 1999), slow vital capacity, Penn upper motor neuron score, and treatment with riluzole were also assessed.

The following data were collected from retrospective review of case-notes: site of onset, revised El Escorial status at diagnosis (Brooks *et al.*, 2000), date of diagnosis, genetic status, and disease course.

Maximal voluntary isometric contraction force of ankle dorsiflexors was measured using a fixed myometry system (Quantitative Muscle Strength Assessment–QMA, Aeverl Medical, Gainesville, GA). Motor unit number and size indices, measures of denervation and reinnervation, respectively, were recorded from ipsilateral tibialis anterior, according to standardised protocols (Neuwirth *et al.*, 2010), using a Dantec Keypoint electromyography machine (Natus Medical, Pleasanton, CA) from the less affected side in patients (to avoid "floor effects"), and from a randomised side in controls. The same leg was tested for all subsequent imaging assessments.

Magnetic resonance imaging and spectroscopy

Hardware

All scans were conducted at 3 Tesla (Philips Ingenia, Philips Healthcare, Best, Netherlands) using a transmit-receive dual-tuned $^{1}H/^{31}P$ birdcage quadrature head-coil (Rapid Biomedical, Würzburg, Germany) for brain, and a transmit-receive ^{31}P surface-coil (Philips Healthcare, Best, Netherlands) for muscle acquisitions.

Sequences

In brain, two-dimensional chemical shift imaging was employed using image-selected *in vivo* spectroscopy (Ordidge *et al.*, 1986; Ordidge *et al.*, 1988) for volume localisation. Spectra were acquired from a coronal slice capturing motor pathways including pre-central gyrus and descending corticospinal and corticobulbar tracts to the brainstem, placed by a single observer according to standardised anatomical landmarks (Fig. 1 A-C). Adiabatic pulses were used and the following acquisition parameters: repetition time=4.0 seconds, echo time=0.26

milliseconds, signal averages=2, sampling points=2048, spectral bandwidth=3000 Hertz, flip angle=90° slice thickness=40 millimetres (mm), field of view=300x300 mm^2, matrix=12x12 yielding a native voxel size of 25x25x40 mm^3 which, after k-space filtering and zero filling, was reconstructed to 21x21x40 mm^3. Spectral signal-to-noise ratio and line shapes were optimised using second-order pencil beam shim and WALTZ-4 broadband heteronuclear decoupling with nuclear Overhauser effect. Fig. 1 D illustrates a representative brain spectrum acquired from the pons.

A T2-weighted spin echo image (repetition time=3 seconds, echo time=80 milliseconds, flip angle=90°, slice thickness=4 mm, field of view=230x230 mm^2, reconstructed matrix=432x432 mm^2, reconstructed voxel size=0.53x0.53x4.00 mm^3) was used to guide anatomical positioning of the spectroscopic grid. A T1-weighted inversion-recovery volumetric image (repetition time=8.4 milliseconds, echo time=3.9 milliseconds, inversion time=1.0 second, flip angle=8°, slice thickness=1 mm, field of view=240x240 mm^2, reconstructed matrix=256x256 mm^2, reconstructed voxel size=0.94x0.94x1.00 mm^3) was acquired for spectroscopic co-localisation and correction for partial volume effects. Brain spectroscopy and imaging acquisition time was approximately 25 minutes.

In muscle, spectra were acquired from the proximal portion of ankle dorsiflexors encompassing tibialis anterior using a Philips surface-coil positioned according to standardised anatomical landmarks. The top of the coil was placed two centimetres below the tibial tuberosity (Fig. 2 B-C). Positioning was carried out by the same personnel for all participants and was cross-checked. This was necessary to ensure consistent sampling across all subjects, as oxidative capacity differs between proximal and distal portions of tibialis anterior (Boss *et al.*, 2018). A pulse-acquire sequence (repetition time=4.5 seconds, echo time=0.09 milliseconds, signal averages=32, sampling points=2048, spectral bandwidth=3000 Hertz, flip angle=90°, adiabatic pulses, WALTZ-4 decoupling, nuclear Overhauser enhancement) was first applied at rest. A

representative muscle spectrum acquired at rest is shown (Fig. 2 A). A dynamic protocol (repetition time=5.0 seconds, echo time=0.09 milliseconds, signal averages=3, sampling points=2048, spectral bandwidth=3000 Hz, flip angle=90°, adiabatic pulses, WALTZ-4 decoupling, nuclear Overhauser enhancement) was then performed: scans were acquired for 2 minutes at resting baseline, followed by 1 minute of supervised isometric ankle dorsiflexion against a load applied using an magnetic resonance-compatible pulley system, then 3 minutes recovery. A load equivalent to a third of the participant's maximal voluntary isometric contraction was applied to minimise changes in pH which may be caused by anaerobic glycolysis recruited at higher forces (Baker *et al.*, 2010; Meyerspeer *et al.*, 2020). An example of a dynamic spectroscopic series is depicted (Fig. 2 E). Muscle spectroscopy acquisition time was approximately 20 minutes.

Spectroscopic data processing

Data from all research participants were anonymised at acquisition, a random study number assigned, and all analyses were conducted on anonymised data by a researcher blinded to participant status.

Signal fitting was performed in the time domain using the non-linear least square advanced method for accurate, robust, and efficient spectral fitting (AMARES) algorithm (available with jMRUI, http://www.jmrui.eu) (Vanhamme *et al.*, 1997; Naressi *et al.*, 2001; Stefan *et al.*, 2009). Signal pre-processing included manual zero and first-order phasing to purely absorptive line shapes and assignment of a frequency shift to 0 parts per million for phosphocreatine. No apodisation was performed. Thirteen and 12 resonances were fitted in brain and muscle, respectively, assuming Lorentzian line shapes (Mierisová and Ala-Korpela, 2001), as shown in Fig. 1 E (brain) and Fig. 2 D (muscle). For γATP and αATP, amplitudes were constrained in 1:1 ratio for each doublet, and 0.5:1:0.5 ratio for the βATP triplet; linewidths of each ATP multiplet were constrained to each other and coupling constants were fixed to 18 Hertz; soft

constraints on linewidth were applied to phosphocreatine (5-20 Hertz) and the remainder of resonances (5-30 Hertz) (de Graaf, 2007; Hattingen *et al.*, 2009). Quality of fit was assessed visually in all cases to exclude spurious signals or baseline distortions, according to recently published consensus (Wilson *et al.*, 2019). Amplitudes were corrected for T1 relaxation effects using published values for brain (Peeters *et al.*, 2019) and muscle (Meyerspeer *et al.*, 2003; Bogner *et al.*, 2009).

T1-weighted volumetric images were segmented using Statistical Parametric Mapping software (SPM12, https://www.fil.ion.ucl.ac.uk/spm/software/spm12/) and co-registered to the spectroscopic grid using MATLAB and Statistics Toolbox Release 2019b (The MathWorks, Inc., Natick, Massachusetts, United States). For each analysed spectroscopic voxel, the partial fraction of brain (grey plus white matter divided by total voxel content) was calculated (Quadrelli *et al.*, 2016). These data were used to test any significant results, to determine whether changes could be attributable to partial volume effects, by entering partial brain fraction as additional covariate into multiple regression models.

Reported parameters

Total phosphorus signal was estimated as the sum of peak amplitudes and used to normalise measured individual resonances in line with previous literature (Kato *et al.*, 1995; Christensen *et al.*, 1996; Hu *et al.*, 2000; Kato *et al.*, 2000; Hamakawa *et al.*, 2004). Intracellular pH and magnesium were calculated from the chemical shift between inorganic phosphate and phosphocreatine, and βATP and phosphocreatine, respectively (Iotti *et al.*, 2000). ADP concentrations and ΔG_{ATP} were calculated according to previously published methods (Iotti *et al.*, 2005). When interpreting ΔG_{ATP}, a negative sign indicates that energy is released from ATP hydrolysis (the reaction is exergonic), whereas absolute ΔG_{ATP} values refer to the amount of useful energy that can be released by ATP hydrolysis. Calculation of ADP requires millimolar expression of ATP, phosphocreatine, and inorganic phosphate. Hence, according to previously

published literature, ATP concentrations in healthy individuals were assumed 3 millimolar in brain (Barbiroli *et al.*, 1993) and 8 millimolar in muscle (Kemp *et al.*, 2007) and mean γATP/total phosphorus signal values recorded in controls were employed as an external reference to derive ATP, phosphocreatine, and inorganic phosphate values in millimolar in each study participant to calculate ADP.

For dynamic muscle data, phosphocreatine recovery constants (k) were calculated for each research participant assuming exponential recovery, using the following formula y=Ye+(Yp-Ye)*(1-exp(-x*k)) (Meyerspeer *et al.*, 2020), where Ye=end-exercise phosphocreatine, Yp=phosphocreatine following recovery, and x=time. An example of phosphocreatine fitting during recovery is illustrated (Fig. 2 F). A sigmoidal curve was fitted to phosphocreatine/inorganic phosphate recovery (Jeneson *et al.*, 1995; Kemp *et al.*, 2007), as illustrated (Fig. 2 G). The Hill coefficient was calculated as a measure of rate of phosphocreatine/inorganic phosphate recovery to baseline. To avoid over-fitting dynamic data in cases of severe weakness, goodness-of-fit of recovery parameters was assessed for each individual time series and R^2 values<0.25 were excluded.

Statistical analyses

Due to the large and multi-dimensional dataset, a hierarchical statistical analysis approach was adopted. Analogous anatomical regions were compared between groups. First, we tested for between-group voxel-wise differences in phosphocreatine, as previous ^{31}P-MRS brain studies in mitochondrial cytopathies have reported this parameter an early indicator of mitochondrial dysfunction (Barbiroli *et al.*, 1993). For any significant voxels, we then assessed all spectral metabolites and calculated ΔG_{ATP} to test our *a priori* hypothesis that bioenergetic dysfunction in ALS may be caused by mismatched cellular energy demand and ATP synthesis resulting from mitochondrial uncoupling/electron transport chain inhibition. Analyses were corrected for multiple comparisons at both voxel-wise and spectral level (Q=0.05) (Benjamini *et al.*,

2006). ΔG_{ATP} is calculated for resting data employing a formula which incorporates individual variations in pH and magnesium, assuming constant free intracellular sodium, potassium, and calcium (Iotti *et al.*, 2005). These assumptions may not be valid during muscle contraction so, for dynamic data, in addition to phosphocreatine, phosphocreatine/inorganic phosphate ratio was reported instead of ΔG_{ATP}, accepting that this ratio reflects only the mitochondrial component of ΔG_{ATP} and might not be fully indicative of cellular bioenergetic status. Any spectroscopic parameters that differed significantly between patients and controls were correlated with relevant clinical measures: revised ALS functional rating scale, slow vital capacity, and upper motor neuron score for brain parameters, and 10-metre walk test, maximal voluntary isometric contraction, motor unit number and size indices for muscle parameters. Regression coefficients (R) with 95% confidence intervals (CI) were reported.

Between-group comparisons for continuous data were conducted using either unpaired two-tailed t-tests with Welch correction (as equality of variance could not always be assumed) or Mann-Whitney U tests, depending on data distribution, assessed using the D'Agostino-Pearson test. For categorical data, chi-squared tests were applied. Statistical significance was considered at $p<0.05$. Multiple comparisons were corrected by false discovery rate ($Q=0.05$) as described above (Benjamini *et al.*, 2006). For any significant voxels, data were then reanalysed adjusting, in turn, for voxel brain tissue fraction and participant age, using multiple linear regression models. Clinical, electrophysiological and radiological associations were assessed using linear regression. Dynamic time series were assessed using two-way repeated measures ANOVA. The effects of interest in dynamic muscle data were between-group differences in each spectroscopic parameter and change in that measure over time, which were assessed from the ANOVA group and measure-time interaction terms, respectively. Interpretation of phosphocreatine recovery relies on the assumption that pH variations over time are within 0.1 units (Meyerspeer *et al.*, 2020); stability of pH over time was reported.

Statistical analysis was performed using GraphPad Prism (version 8.3.0 for Windows, GraphPad Software, San Diego, California USA, www.graphpad.com).

Data availability

Anonymised data will be shared for reasonable requests from qualified investigators.

Results

Participants' clinical and neurophysiological characteristics

Demographic, clinical, and neurophysiological characteristics of the 30 research participants are summarised (table 1). Patients and controls were matched for age, gender, and weight. Two patients could not perform the 10-metre walk test due to advanced weakness, and no neurophysiological parameters could be acquired from one of these patients because compound muscle action potentials were unrecordable. Symptom onset was bulbar in four patients, six had upper limb-onset and 10 lower limb-onset). El Escorial status at diagnosis was: 17 clinically probable (six laboratory-supported), two clinically possible, and one definite ALS. Median interval between symptom onset and diagnosis was 13 months. Three patients had familial disease: two had confirmed *C9orf72* repeat expansions and the third declined genetic testing. In all patients, disease course was consistent with ALS.

Brain phosphorus-31 magnetic resonance spectroscopy

Differences between ALS patients and healthy controls were found only in the brainstem, in the pontine region (corresponding to the voxel highlighted in yellow in Fig. 1 A and B) and are summarised in table 2. Between-group differences in ΔG_{ATP} and phosphocreatine retained significance after adjusting for partial brain fraction within the voxel (ΔG_{ATP}: estimate=2.04, CI=0.50 to 3.59, p=0.012; phosphocreatine: estimate=-0.04, CI=-0.07 to -0.01, p=0.008) and age (ΔG_{ATP}: estimate=1.94, CI=0.41 to 3.46, p=0.015; phosphocreatine: estimate=-0.04, CI=-

0.07 to -0.01, p=0.012). The significance of ADP in adjusted models both for partial brain fraction (estimate=93.71, CI=-9.93 to 197.30, p=0.074) and age (estimate=85.67, CI=-13.74 to 185.10, p=0.088) became weaker. Neither partial brain fraction nor age regressors were statistically significant in these adjusted models (brain fraction in ΔG_{ATP} model: estimate=-1.03, CI=-8.40 to 6.34, p=0.774; brain fraction in phosphocreatine model: estimate=-0.002, CI=-0.13 to 0.13, p=0.977; brain fraction in ADP model: estimate=47.86, CI=-447.20 to 542.90, p=0.843; age in ΔG_{ATP} model: estimate=0.02, CI=-0.05 to 0.08, p=0.648; age in phosphocreatine model: estimate=-0.0004, CI=-0.002 to 0.001, p=0.476; age in ADP model: estimate=2.61, CI=-1.82 to 7.03, p=0.234). In patients, in the brainstem, lower phosphocreatine was associated with greater disability on revised ALS functional rating scale (R=0.54, CI=0.11 to 0.80, p=0.017) and lower slow vital capacity (R=0.59, CI=0.18 to 0.82, p=0.008), but there was no association with upper motor neuron score (R=0.31, CI=-0.20 to 0.68, p=0.223). Higher ADP concentrations were associated with greater disability on revised ALS functional rating scale (R=-0.58, CI=-0.84 to -0.09, p=0.024) and lower slow vital capacity (R=-0.52, CI=-0.82 to -0.02, p=0.045), but not with upper motor neuron score (R=-0.38, CI=-0.77 to 0.22, p=0.207). ΔG_{ATP} did not correlate with any of the clinical parameters assessed.

No differences between patients and controls were detected in other brain regions. No statistically significant differences were found in total phosphorus signal between patients and controls in any voxel. Of the 330 spectra analysed, 10 were rejected on technical grounds, based on the criteria outlined in the methods section, prior to statistical analysis. No between-group differences were found in partial brain fraction of the pontine voxel: control mean=0.61 (standard deviation=0.12), patient mean=0.62 (standard deviation=0.10), difference (patients-controls)=0.02, CI=-0.08 to 0.11, p=0.744.

Skeletal muscle phosphorus-31 magnetic resonance spectroscopy: rest acquisition

Spectroscopic results from tibialis anterior are summarised in table 3.

In patients, reduced absolute values of ΔG_{ATP} were associated with slower walking speed (R=0.49, CI=0.03 to 0.78, p=0.039), there was no significant correlation with maximal voluntary isometric contraction (R=-0.41, CI=-0.73 to 0.06, p=0.082), but reduced absolute values of ΔG_{ATP} were associated with lower motor unit number index (R=-0.58, CI=-0.82 to -0.17, p=0.010). There was no association with motor unit size index (R=0.144, CI=-0.33 to 0.56, p=0.556). Higher inorganic phosphate was associated with reduced walking speed (R=0.77, CI=0.46 to 0.91, p<0.001), greater weakness on maximal voluntary isometric contraction (R=-0.57, CI=-0.81 to -0.15, p=0.012), and lower motor unit number index (R=-0.77, CI=-0.91 to -0.49, p<0.001). No association was found with motor unit size index (R=0.30, CI=-0.18 to 0.66, p=0.221). Higher phosphomonoesters were associated with reduced walking speed (R=0.66, CI=0.28 to 0.86, p=0.003), greater weakness on maximal voluntary isometric contraction (R=-0.53, CI=-0.79 to -0.10, p=0.020), and lower motor unit number index (R=-0.55, CI=-0.80 to -0.13, p=0.015). No association was found with motor unit size index (R=0.01, CI=-0.45 to 0.46, p=0.977). pH and magnesium did not correlate with any of the clinical and neurophysiological measures.

No statistically significant difference was found in total phosphorus signal between patients and controls in tibialis anterior. All spectra were of sufficient quality to allow accurate fitting.

Skeletal muscle phosphorus-31 magnetic resonance spectroscopy: dynamics

Phosphocreatine/inorganic phosphate ratio, γATP, phosphocreatine, and inorganic phosphate dynamics are shown (Fig. 3). On submaximal contraction, no statistically significant differences were found in the ANOVA measure-time interaction term for phosphocreatine/inorganic phosphate ratio (Fig. 3 A), γATP (Fig. 3 B), phosphocreatine (Fig.

3 C), and inorganic phosphate (Fig. 3 D) dynamic curves, although statistically significant between-group differences were found in phosphocreatine/inorganic phosphate ratio (p=0.010) and inorganic phosphate (p=0.004) dynamics. The phosphocreatine/inorganic phosphate ratio Hill coefficient was decreased in patients (mean=1.23 standard deviation=0.73) compared to controls (mean=2.20 standard deviation=1.10, CI=-1.94 to -0.02, p=0.047) indicating slower phosphocreatine/inorganic phosphate ratio recovery in ALS. At the end of muscle contraction, mean ATP increased by 4.40% of baseline values in controls, but decreased by 2.21% in patients (controls' standard deviation=7.44%, patients' standard deviation=8.40%, CI=-12.94 to -0.28, p=0.042). No statistically significant changes were found in phosphocreatine recovery constants (controls' mean=2.26 $minutes^{-1}$ standard deviation=1.24, patients' mean=2.23 $minutes^{-1}$ standard deviation=2.87, p=0.269). One patient could not perform the dynamic protocol due to advanced weakness. R^2 of six phosphocreatine/inorganic phosphate ratios and eight phosphocreatine recovery dynamics were below 0.25 and were, hence, excluded prior to conducting statistical analysis of recovery constants. pH remained stable throughout recovery (<0.1 unit variation); pH dynamics are reported in supplementary material.

Discussion

This paper is the first to demonstrate evidence of mitochondrial dysfunction both in brain and muscle tissue *in vivo* in ALS. The results are clinically and neurophysiologically relevant, represent an important step towards stratifying patients by disease mechanism, and offer new insights into pathophysiology. Such steps are necessary to target mitochondrial dysfunction for therapeutic benefit in the future.

Central mitochondrial dysfunction in amyotrophic lateral sclerosis is clinically relevant and characterised by decreased phosphocreatine

The spectroscopic signature in the brainstem in ALS (i.e. decreased ΔG_{ATP} and phosphocreatine with unchanged ATP) has been previously described in the brain in mitochondrial cytopathies (Eleff *et al.*, 1990; Barbiroli *et al.*, 1993; Lodi *et al.*, 1994; Barbiroli *et al.*, 1995a; Barbiroli *et al.*, 1995b) and is consistent with primary mitochondrial dysfunction. Decreased ΔG_{ATP} indicates that, despite preserved ATP levels, relatively less work can be generated through ATP hydrolysis. Changes in ΔG_{ATP} appear to be predominantly driven by decreased phosphocreatine, which might be expected as brain bioenergetic function is regulated by the creatine-phosphocreatine system, and is crucial in ensuring adequate ATP levels during action potentials (Andres *et al.*, 2008). When the electron transport chain is impaired, resting ATP is maintained at the expense of the phosphocreatine buffer. Our data indicate that buffering capacity is reduced, suggesting deficits in both fast and more sustained ATP generation in ALS. We also detected increases in ADP, consistent with electron transport chain impairment, although this result was statistically less robust than phosphocreatine and did not survive correction for multiple comparisons. Associations between phosphocreatine with slow vital capacity and revised ALS functional rating scale suggest that the identified mitochondrial dysfunction contributes to clinically relevant pathophysiology.

We only detected bioenergetic dysfunction in the brainstem and not in cortical and deep white matter motor regions. This did not appear attributable to over-representation of bulbar disease in our cohort, rather it could reflect the compressed functional anatomy of this region, where all corticospinal tract and most corticobulbar tract axons are located. A proton magnetic resonance spectroscopy study in ALS showed reductions in N-acetylaspartate (synthesised primarily in mitochondria (Patel and Clark, 1979)), particularly in this region (Bradley *et al.*, 1999). Defective retrograde axonal transport also occurs in ALS and dysfunctional

mitochondria may accumulate along axons leading to a relative increase in the number measured per unit area (De Vos and Hafezparast, 2017). *Post-mortem* studies have shown reduced electron transport chain complex activity in lower segments of corticomotor tracts (Fujita *et al.*, 1996; Borthwick *et al.*, 1999; Wiedemann *et al.*, 2002), but no changes in oxidative phosphorylation in motor cortex (Bowling *et al.*, 1993; Browne *et al.*, 1998). Although brain atrophy has been reported in ALS (Ellis *et al.*, 2001; De Marco *et al.*, 2015; de Albuquerque *et al.*, 2017), it is considered unlikely that technical factors such as differential partial volume effects contributed to spectroscopic differences between patients and controls in this study, because adding partial brain fraction as a covariate to regression analyses did not significantly alter the overall pattern of results (slightly weaker significance in ADP notwithstanding), there were no differences in partial brain fraction between patients and controls in the brainstem voxel, the normalisation method we used is extremely robust to such potential biases (Klunk *et al.*, 1994; de Graaf, 2007), and ^{31}P-MRS is less susceptible to this artefact than proton spectroscopy because concentrations of phosphorus metabolites in CSF (in contrast to water) are negligible (Jellinger, 2009). It is also important to consider whether age could potentially have influenced results, but our patient and control groups appeared well-matched and, in an age-adjusted regression models, the overall pattern and direction of between-group differences remained consistent with primary mitochondrial dysfunction, whilst age was not significant in any of the adjusted models, suggesting that any such effect was minor.

Peripheral mitochondrial dysfunction in amyotrophic lateral sclerosis is clinically relevant and characterised by elevated inorganic phosphate

We also identified bioenergetic dysfunction in ALS in muscle, both at rest and following exercise. A single previous ^{31}P-MRS study investigating the metabolic effects of denervation in various conditions, including ALS, showed similar changes in forearm muscles (Zochodne *et*

al., 1988). Two previous small studies investigated tibialis anterior, one in five patients and five controls (Sharma *et al.*, 1995), the other in six patients and six controls (Kent-Braun and Miller, 2000), and no significant changes in phosphocreatine, inorganic phosphate, phosphocreatine/inorganic phosphate ratio or phosphocreatine recovery were detected; ΔG_{ATP} was not studied. We selected tibialis anterior as it appears particularly sensitive to T2-weighted signal changes in ALS (Jenkins *et al.*, 2018). As in brain, reduced ΔG_{ATP} was evident in patients at rest, indicating decreased free energy available following ATP hydrolysis. In skeletal muscle, ΔG_{ATP} reflects sarcoplasmic energy demand and acts as a signal to regulate mitochondrial oxidative phosphorylation (Kemp *et al.*, 2007). Specifically, the products of ATP hydrolysis (ADP and inorganic phosphate) increase at times of elevated cellular energy demand and ATP and phosphocreatine production is stimulated through the electron transport chain to re-establish physiological ΔG_{ATP} values (Kemp *et al.*, 2007; Wu *et al.*, 2007). However, the mechanism for the ΔG_{ATP} decrease appeared different in muscle to brain, predominantly associated with increased inorganic phosphate levels and preserved phosphocreatine. Mitochondria in diseased muscle appear less responsive to increased inorganic phosphate, although mitochondrial dysfunction may be less severe than in brain, because phosphocreatine reserves are not substantially depleted. These results may reflect differences in the tissue measured. In ALS, TDP-43 burden is located in upper and lower motor neurons (Neumann *et al.*, 2006), whilst changes in muscle may be secondary to denervation. It is not possible to determine from this study whether the bioenergetic metabolic signature of ALS differs from other denervating or primary muscle diseases or represents a non-specific secondary effect (Dinh *et al.*, 2009; Gramegna *et al.*, 2018).

It is possible that intracellular inorganic phosphate redistribution from mitochondrial matrix to the sarcoplasm contributes to our results. Intra-mitochondrial inorganic phosphate is not visible on the ^{31}P-MRS sequence we employed and inorganic phosphate transport into mitochondrial

matrix is driven by the pH gradient across the inner mitochondrial membrane (Ferreira and Pedersen, 1993). A decrease in mitochondrial pH gradient would reduce import of inorganic phosphate to stimulate the electron transport chain, causing a relative increase in the cytoplasm, detectable with ^{31}P-MRS. Reduced mitochondrial pH gradient can result from mitochondrial uncoupling and/or electron transport chain complex I to IV inhibition (Nicholls, 2013). Studies in several cellular and animal ALS models, and patient material, have found deficits in electron transport chain complexes and in mitochondrial membrane potential (Vandoorne *et al.*, 2018). Lastly, sarcolemmal permeability to inorganic phosphate is affected by hormones such as insulin, which increase muscle inorganic phosphate uptake (Petersen *et al.*, 2005). Although denervation can be associated with skeletal muscle insulin resistance (Burant *et al.*, 1984), this would result in decreased inorganic phosphate; additionally, no research participant had diabetes mellitus or a pre-diabetic state; hence alterations in sarcolemmal permeability are considered less likely. Reduced ΔG_{ATP} may therefore represent indirect evidence for electron transport chain impairment, with a signature of reduced mitochondrial reactivity to signals of elevated cytoplasmic energy demand.

Alterations in phosphomonoesters in amyotrophic lateral sclerosis skeletal muscle are linked to bioenergetic dysfunction

We detected an increase in phosphomonoesters in patients which correlated with slower walking speed, lower maximal voluntary isometric contraction and lower motor unit number index, indicating clinical relevance and association with denervation. Phosphomonoesters are used to synthesise cell membranes and are often elevated in rapidly proliferating tissues, such as malignancies (Redmond *et al.*, 1992; Valkovič *et al.*, 2017). In our study, phosphomonoesters did not correlate with motor unit size index, suggesting that accelerated membrane synthesis associated with reinnervation was not the cause. This appears different to the spectroscopic signature of primary muscle disease, such as muscular dystrophies, in which

phospholipid catabolites (phosphodiesters) accumulate possibly as a consequence of tissue remodelling (Hooijmans *et al.*, 2017a; Hooijmans *et al.*, 2017b).

Phospholipid synthesis requires efficient energy-dependent transfer of phosphomonoesters between mitochondria and endoplasmic reticulum (Vance, 2015). Hence, it is possible that ALS-related bioenergetic impairment and/or aberrant endoplasmic reticulum-mitochondrial contact causes phosphomonoesters to accumulate. Mitochondrial membrane replenishment is required to maintain efficient ATP production especially in conditions of increased oxidative stress, such as ALS (Kowaltowski and Vercesi, 1999; Barber and Shaw, 2010). These explanations are supported by a *post-hoc* analysis which showed that higher phosphomonoesters correlated with lower absolute values of ΔG_{ATP} (R=0.68, CI=0.34 to 0.86, p=0.0009), linking bioenergetic dysfunction to altered membrane metabolism.

Alterations in pH and intracellular magnesium are detected in amyotrophic lateral sclerosis skeletal muscles

The pH increase in patients is consistent with reduced anaerobic glycolysis (resulting in lactate production and decreasing pH). ~~This may be reflective of selective vulnerability of motor neurons innervating glycolytic muscle fibres, which tend to be lost in the earlier stages of MND (Ragagnin et al., 2019).~~ We also detected lower free magnesium concentrations in ALS muscle, which may be secondary to denervation (Shimizu and Kuriaki, 1960). Magnesium is important for ATP synthase function (Ko *et al.*, 1999) and cytoplasmic concentration is regulated by complex interplay of cytosolic buffering, sarcolemmal transport, and mitochondrial sequestration (Murphy, 2000).

Dynamic protocol demonstrates impaired recovery of phosphocreatine/inorganic phosphate ratio

Phosphocreatine/inorganic phosphate ratio recovery was substantially reduced in the ALS cohort. Slower phosphocreatine/inorganic phosphate ratio recovery is consistent with findings in resting muscle and suggests that mitochondria are less responsive to increased cytoplasmic energy demands, possibly consequent to altered inorganic phosphate metabolism. The observed relative decline in ATP during muscle contraction in patients compared to controls further supports this hypothesis. No statistically significant differences in phosphocreatine recovery were evident. Phosphocreatine re-synthesis is fully dependent on mitochondrial oxidative phosphorylation and often used as a measure of oxidative capacity, provided that pH remains constant throughout recovery (Meyerspeer *et al.*, 2020), which was the case in our experiments. Our data suggest that ATP synthase activity was not substantially impaired, although interpretation must be cautious because a number of phosphocreatine recovery constants had to be rejected due to poor fitting (R^2<0.25).

Taken together, these data illustrate the multi-faceted nature of bioenergetic impairment in ALS skeletal muscle which appears distinct from CNS changes.

Limitations and future directions

The small cohort size and cross-sectional design are limitations of this study. Replication of our findings in a larger longitudinal study is necessary to determine whether the identified changes are sensitive to disease progression and so act as a marker of target engagement for future therapeutic agents targeting bioenergetic pathways. Another limitation is the lack of disease controls, which precludes assessment of disease specificity of detected changes. Hence our findings are preliminary, pending investigation in subjects with other denervating diseases or myopathies.

Nonetheless, this study provides an important first demonstration that bioenergetic dysfunction is detectable *in vivo* even in small cohorts of ALS patients and appears clinically important, with potential practical implications for patient stratification. For instance, elevated basal energy expenditure observed in approximately fifty percent of patients (Desport *et al.*, 2001; Bouteloup *et al.*, 2009; Funalot *et al.*, 2009) is associated with worse prognosis (Desport *et al.*, 2005; Steyn *et al.*, 2018). This hypermetabolic state is paradoxical when reduced mobility, muscle bulk, and caloric intake in ALS all decrease basal energetic requirements; the cause is currently unclear (Ferri and Coccurello, 2017). Structural (Gorges *et al.*, 2017) and humoral (Ahmed *et al.*, 2019) influences and cellular mitochondrial dysfunction with electron transport chain uncoupling (Dupuis *et al.*, 2003; Dupuis *et al.*, 2009) have been proposed. Associations between greater physical activity and development of ALS have been investigated (Harwood *et al.*, 2016; Lacorte *et al.*, 2016). Hypotheses of abnormal bioenergetic adaptation to exercise could be investigated *in vivo* in future ^{31}P-MRS studies. Future studies could combine this technique with other imaging modalities, already being applied in ALS (Pioro, 1997; Pioro *et al.*, 1999; Ratai *et al.*, 2018; Kalra, 2019) and histopathology to further explore mechanistic hypotheses including links with patients' systemic metabolic status.

In summary, this is the first study to demonstrate evidence of clinically and neurophysiologically relevant mitochondrial dysfunction *in vivo* in brain and skeletal muscle in ALS. ΔG_{ATP} was reduced in both tissues, despite preserved ATP levels, and mechanisms differed according to tissue: in brain, phosphocreatine buffering was reduced, whereas in muscle mitochondria appeared insensitive to elevated inorganic phosphate, despite preserved phosphocreatine. Alterations in phosphomonoesters, pH, and magnesium were also detected in muscle. These results offer novel insights into ALS pathophysiology representing a new step towards stratifying patients by disease mechanism, to target mitochondrial dysfunction for future therapeutic benefit.

Acknowledgments

We thank research participants, Yasmin Feuozi-Akhtiary for contributing to data analysis, and Julia Bigley for helping with scanning.

Funding

This work was supported by: NIHR Sheffield Biomedical Research Centre for Translational Neuroscience (IS-BRC-1215-20017), British Medical Association Vera Down, and Neurocare/Ryder Briggs Trust. The views expressed are those of the authors and not necessarily those of the NHS, the NIHR, or the Department of Health and Social Care. PJS is supported as an NIHR Senior Investigator (NF-SI-0617-10077).

Competing interests

The authors report no competing interests relevant to this work.

Supplementary material

Supplementary material is available at *Brain* online.

Tables and figure legends

Table 1 Participants' characteristics at time of scan.

	Controls *mean (±standard deviation)*	***Patients*** *mean (±standard deviation)*	***Means' difference*** *Patients-controls (±SEM)*	***t, DF***	***95% confidence interval***	***p***
Number of participants	10	20	*NA*	*NA*	*NA*	*NA*
Age (years)	57.30 (±10.90)	62.45 (±12.36)	5.15 (±4.42)	1.17, 20.32	-4.06 to 14.36	*0.257*
Gender	5 F : 5 M	7 F : 13 M	*NA*	*NA*	*NA*	*0.429*
Weight (Kilograms)	72.40 (±14.27)	74.50 (±12.31)	2.10 (±5.28)	0.40, 15.90	-9.11 to 13.31	*0.696*
10-metre walk test (seconds)	**4.45 (±0.61)**	**8.73 (±3.73)**	**4.28 (±0.90)**	**4.75, 18.77**	**2.39 to 6.17**	***<< 0.001****
Positive history of diabetes mellitus or pre-diabetes	none	none	*NA*	*NA*	*NA*	*NA*
Disease duration (months)	NA	29.04 (±24.36)	*NA*	*NA*	*NA*	*NA*
Revised ALS functional rating scale	NA	36.95 (±5.22)	*NA*	*NA*	*NA*	*NA*
Slow vital capacity (% predicted)	NA	85.60 (±22.85)	*NA*	*NA*	*NA*	*NA*
Upper motor neuron score	NA	10.22 (±2.92)	*NA*	*NA*	*NA*	*NA*
On riluzole	NA	16	*NA*	*NA*	*NA*	*NA*
Maximal voluntary isometric contraction (Kilograms)	**13.15 (±2.21)**	**8.25 (±5.68)**	***NA***	***NA***	***NA***	***0.002#****
Compound muscle action potential (millivolts)	**4.84 (±0.86)**	**3.37 (±1.34)**	**-1.48 (±0.41)**	**3.60, 25.76**	**-2.32 to -0.63**	***0.001****
Motor unit number index	**109.70 (±23.98)**	**66.67 (±29.54)**	**-43.00 (±10.17)**	**4.23, 22.07**	**-64.09 to -21.91**	***<< 0.001****
Motor unit size index (microvolts)	**44.67 (±4.62)**	**51.96 (±8.98)**	***NA***	***NA***	***NA***	***0.014#****

A chi-squared test was employed to test for gender matching, Mann-Whitney U test was applied in comparisons indicated by the hash symbol, for all other between-group comparisons, unpaired two-tailed t-tests with Welch correction were conducted. Asterisks indicate p values

that remained significant after multiple comparisons correction. DF=Welch corrected degrees of freedom, F=female, M=male, NA=not applicable, SEM=standard error of mean.

Table 2 Spectroscopic parameters measured in the pons.

	Controls *mean (±standard deviation)*	***Patients*** *mean (±standard deviation)*	***Means' difference*** *Patients-controls (±SEM)*	***t, DF***	***95% confidence interval***	***p***
ΔG_{ATP} (kilojoule/mole)	**-61.12 (±1.88)**	**-59.12 (±1.56)**	***2.00 (±0.75)***	***2.68, 14.53***	***0.40 to 3.59***	***0.018***
γATP	0.15 (±0.03)	0.16 (±0.04)	*0.01 (±0.01)*	*0.43, 24.44*	*-0.02 to 0.04*	*0.668*
Phosphocreatine	**0.25 (±0.02)**	**0.21 (±0.04)**	**-0.04 (±0.01)**	**3.42, 26.44**	**-0.07 to -0.02**	***0.002****
Adenosine diphosphate (micromolar)	**169.60 (±64.85)**	**265.50 (±132.80)**	***95.86 (±40.53)***	***2.37, 21.42***	***11.68 to 180.00***	***0.028***
Inorganic phosphate	0.08 (±0.04)	0.09 (±0.04)	*0.02 (±0.02)*	*1.06, 17.29*	*-0.02 to 0.05*	*0.303*
pH	7.14 (±0.11)	7.07 (±0.07)	*-0.07 (±0.04)*	*1.70, 13.29*	*-0.15 to 0.02*	*0.113*
Free magnesium (millimolar)	0.13 (±0.05)	0.14 (±0.06)	*0.01 (±0.02)*	*0.59, 17.89*	*-0.03 to 0.06*	*0.563*
Phosphomonoesters	0.20 (±0.05)	0.18 (±0.04)	*-0.02 (±0.02)*	*1.15, 13.81*	*-0.06 to 0.02*	*0.270*
Phosphodiesters	0.17 (±0.04)	0.19 (±0.05)	*0.02 (±0.02)*	*1.32, 21.97*	*-0.01 to 0.06*	*0.199*

Unpaired two-tailed t-tests with Welch correction were conducted in all cases. Asterisks indicate values that remained significant after multiple comparisons correction. DF=Welch corrected degrees of freedom, SEM=standard error of mean, ΔG_{ATP}=Gibbs free energy of ATP hydrolysis (negative sign indicates that ATP hydrolysis is exergonic, amount of energy released is indicated by absolute ΔG_{ATP} values). γATP, phosphocreatine, inorganic phosphate, phosphomonoesters, and phosphodiesters are expressed as a proportion of total phosphorus signal.

Table 3 Spectroscopic parameters measured in tibialis anterior at rest.

	Controls *mean (±standard deviation)*	***Patients*** *mean (±standard deviation)*	***Means' difference*** *Patients-controls (±SEM)*	***t, DF***	***95% confidence interval***	***p***
ΔG_{ATP} (kilojoule/mole)	**-63.56 (±1.02)**	**-62.33 (±1.77)**	**NA**	**NA**	**NA**	***0.028#****
γATP	0.12 (±0.02)	0.12 (±0.02)	NA	NA	NA	*0.214#*
Phosphocreatine	0.56 (±0.02)	0.55 (±0.04)	-0.02 (±0.01)	1.78, 26.71	-0.04 to 0.00	*0.087*

Adenosine diphosphate (micromolar)	19.97 (±7.80)	35.78 (±32.34)	NA	NA	NA	*0.061#*
Inorganic phosphate	**0.06 (±0.01)**	**0.08 (±0.02)**	**0.02 (±0.01)**	**3.49, 27.45**	**0.01 to 0.03**	***0.002****
pH	**6.93 (±0.02)**	**6.96 (±0.03)**	**0.03 (±0.01)**	**2.96, 26.12**	**0.01 to 0.05**	***0.007****
Free magnesium (millimolar)	**0.43 (±0.11)**	**0.34 (±0.12)**	**NA**	**NA**	**NA**	***0.011#****
Phosphomonoesters	**0.02 (±0.01)**	**0.03 (±0.01)**	**0.01 (±0.00)**	**3.52, 27.73**	**0.00 to 0.02**	***0.002****
Phosphodiesters	0.07 (±0.02)	0.06 (±0.02)	-0.01 (±0.01)	1.01, 19.01	-0.02 to 0.01	*0.327*
NAD(P)H+NAD(P)⁺	0.01 (±0.00)	0.01 (±0.01)	0.00 (±0.00)	1.16, 20.50	-0.01 to 0.00	*0.260*

Mann-Whitney U test was applied in comparisons indicated by the hash symbol, for all other between-group comparisons unpaired two-tailed t-tests with Welch correction were conducted. Asterisks indicate values that remained significant after multiple comparisons correction. DF=Welch corrected degrees of freedom, NAD(P)H+NAD(P)⁺=nicotinamide adenine dinucleotides, SEM=standard error of mean, ΔG_{ATP}=Gibbs free energy of ATP hydrolysis (negative sign indicates that ATP hydrolysis is exergonic, amount of energy released is indicated by absolute ΔG_{ATP} values). γATP, phosphocreatine, inorganic phosphate, phosphomonoesters, phosphodiesters, and NAD(P)H+NAD(P)⁺ are expressed as a proportion of total phosphorus signal.

Figure 1 Anatomical localisation of the spectroscopic grid and example of fit of a brain spectrum acquired from the pons in a control.

Coronal (A), sagittal (B), and axial (C) images illustrate positioning of the spectroscopic grid encompassing motor cortex, descending corticospinal and corticobulbar tracts, and the pons. Voxels encompassing motor regions analysed in this study are depicted in blue and yellow in A. An example of a brain spectrum (D) acquired from the pons (voxel highlighted in yellow in A and B); resolved peaks are (from left to right): phosphomonoesters (PME – comprising phosphocholine and phosphoethanolamine peaks), inorganic phosphate (Pi), phosphodiesters (PDE - comprising glycerophosphoethanolamine and glycerophosphocholine), phosphocreatine (PCr), and the γ, α, and β phosphates of ATP. (E) illustrates spectral fitting: in the upper graph the estimated spectrum (in purple) is superimposed on to the raw data; in the graph below, individual resonances are depicted (1=phosphocholine; 2=phosphoethanolamine; 3=Pi; 4=glycerophosphoethanolamine; 5=glycerophosphocholine; 6=PCr; 7 and 8=γATP; 9 and 10=αATP; 11,12, and 13=βATP. Notably, γ and α ATP phosphates resonate as doublets and βATP as a triplet).

Figure 2 Anatomical localisation of muscle spectroscopy, example of fit of a muscle spectrum in a control, and dynamic muscle series.

In (A), a representative muscle spectrum acquired from a control's tibialis anterior at rest is illustrated. Resolved peaks are (from left to right): phosphomonoesters (PME), inorganic phosphate (Pi), phosphodiesters (PDE), phosphocreatine (PCr), γ and α resonances of adenosine triphosphate (ATP), nicotinamide adenine dinucleotides (NAD(P)⁺ and NAD(P)H), and β ATP. Localisation is depicted in B and C, the shimming box is depicted in red. (D) illustrates spectral fitting: in the upper graph the estimated spectrum (in purple) is superimposed on to the raw muscle data; in the graph below, individual resonances are

depicted (1=Pi; 2=PDE; 3=PCr; 4 and 5=γATP; 6 and 7=αATP; 8= NAD(P)$^+$ and NAD(P)H; 9, 10, and 11=βATP; 12=PME. Notably, γ and α ATP phosphates resonate as doublets and βATP as a triplet). (E) illustrates a dynamic time series: phosphocreatine drops substantially upon muscle contraction and gradually recovers to baseline values on cessation of exercise. Representative fitting of phosphocreatine/total phosphorus signal (F) and phosphocreatine/inorganic phosphate ratio (G) recovery values following cessation of exercise, the red lines represent error bars.

Figure 3 Dynamic time series depicting changes in metabolites in tibialis anterior following submaximal muscle contraction in controls (blue) and patients (red). *Contraction begins at minute two and ends at minute three. All experiments were conducted at third of maximal voluntary isometric contraction force. Two-way repeated measures ANOVA statistics are reported below each graph. (A) Phosphocreatine/inorganic phosphate dynamics in patients and controls. (B) γ-adenosine triphosphate dynamics in patients and controls. (C) Phosphocreatine dynamics in patients and controls. (D) Inorganic phosphate dynamics in patients and controls. γATP, phosphocreatine, and inorganic phosphate are expressed as a proportion of total phosphorus signal.*

References

Ahmed RM, Phan K, Highton-Williamson E, Strikwerda-Brown C, Caga J, Ramsey E*, et al.* Eating peptides: biomarkers of neurodegeneration in amyotrophic lateral sclerosis and frontotemporal dementia. Ann Clin Transl Neurol 2019; 6(3): 486-95.

Al-Chalabi A, Calvo A, Chio A, Colville S, Ellis CM, Hardiman O*, et al.* Analysis of amyotrophic lateral sclerosis as a multistep process: a population-based modelling study. Lancet Neurol 2014; 13(11): 1108-13.

Al-Chalabi A, Hardiman O. The epidemiology of ALS: a conspiracy of genes, environment and time. Nat Rev Neurol 2013; 9(11): 617-28.

Andres RH, Ducray AD, Schlattner U, Wallimann T, Widmer HR. Functions and effects of creatine in the central nervous system. Brain Research Bulletin 2008; 76(4): 329-43.

Baker JS, McCormick MC, Robergs RA. Interaction among Skeletal Muscle Metabolic Energy Systems during Intense Exercise. Journal of Nutrition and Metabolism 2010; 2010: 905612.

Barber SC, Shaw PJ. Oxidative stress in ALS: key role in motor neuron injury and therapeutic target. Free Radic Biol Med 2010; 48(5): 629-41.

Barbiroli B, Medori R, Tritschler HJ, Klopstock T, Seibel P, Reichmann H*, et al.* Lipoic (thioctic) acid increases brain energy availability and skeletal muscle performance as shown by in vivo 31P-MRS in a patient with mitochondrial cytopathy. J Neurol 1995a; 242(7): 472-7.

Barbiroli B, Montagna P, Cortelli P, Iotti S, Lodi R, Barboni P*, et al.* Defective brain and muscle energy metabolism shown by in vivo 31P magnetic resonance spectroscopy in nonaffected carriers of 11778 mtDNA mutation. Neurology 1995b; 45(7): 1364.

Barbiroli B, Montagna P, Martinelli P, Lodi R, Iotti S, Cortelli P*, et al.* Defective Brain Energy Metabolism Shown by in vivo 31P MR Spectroscopy in 28 Patients with Mitochondrial Cytopathies. Journal of Cerebral Blood Flow & Metabolism 1993; 13(3): 469-74.

Bartolome F, Wu H-C, Burchell VS, Preza E, Wray S, Mahoney CJ*, et al.* Pathogenic VCP mutations induce mitochondrial uncoupling and reduced ATP levels. Neuron 2013; 78(1): 57-64.

Benjamini Y, Krieger AM, Yekutieli D. Adaptive linear step-up procedures that control the false discovery rate. Biometrika 2006; 93(3): 491-507.

Bogner W, Chmelik M, Schmid AI, Moser E, Trattnig S, Gruber S. Assessment of (31)P relaxation times in the human calf muscle: a comparison between 3 T and 7 T in vivo. Magnetic resonance in Medicine 2009; 62(3): 574-82.

Borthwick GM, Johnson MA, Ince PG, Shaw PJ, Turnbull DM. Mitochondrial enzyme activity in amyotrophic lateral sclerosis: implications for the role of mitochondria in neuronal cell death. Annals of neurology 1999; 46(5): 787-90.

Boss A, Heskamp L, Breukels V, Bains LJ, van Uden MJ, Heerschap A. Oxidative capacity varies along the length of healthy human tibialis anterior. J Physiol 2018; 596(8): 1467-83.

Bouteloup C, Desport JC, Clavelou P, Guy N, Derumeaux-Burel H, Ferrier A*, et al.* Hypermetabolism in ALS patients: an early and persistent phenomenon. Journal of Neurology 2009; 256(8): 1236-42.

Bowling AC, Schulz JB, Brown RH, Jr., Beal MF. Superoxide dismutase activity, oxidative damage, and mitochondrial energy metabolism in familial and sporadic amyotrophic lateral sclerosis. Journal of neurochemistry 1993; 61(6): 2322-5.

Bradley WG, Bowen BC, Pattany PM, Rotta F. 1H-magnetic resonance spectroscopy in amyotrophic lateral sclerosis. J Neurol Sci 1999; 169(1-2): 84-6.

Brooks BR, Miller RG, Swash M, Munsat TL. El Escorial revisited: revised criteria for the diagnosis of amyotrophic lateral sclerosis. Amyotroph Lateral Scler Other Motor Neuron Disord 2000; 1(5): 293-9.

Browne SE, Bowling AC, Baik MJ, Gurney M, Brown RH, Jr., Beal MF. Metabolic dysfunction in familial, but not sporadic, amyotrophic lateral sclerosis. J Neurochem 1998; 71(1): 281-7.

Burant CF, Lemmon SK, Treutelaar MK, Buse MG. Insulin resistance of denervated rat muscle: a model for impaired receptor-function coupling. American Journal of Physiology-Endocrinology and Metabolism 1984; 247(5): E657-E66.

Burstein SR, Valsecchi F, Kawamata H, Bourens M, Zeng R, Zuberi A*, et al.* In vitro and in vivo studies of the ALS-FTLD protein CHCHD10 reveal novel mitochondrial topology and protein interactions. Hum Mol Genet 2018; 27(1): 160-77.

Cedarbaum JM, Stambler N, Malta E, Fuller C, Hilt D, Thurmond B*, et al.* The ALSFRS-R: a revised ALS functional rating scale that incorporates assessments of respiratory function. BDNF ALS Study Group (Phase III). Journal of the neurological sciences 1999; 169(1-2): 13-21.

Chiò A, Calvo A, Mazzini L, Cantello R, Mora G, Moglia C*, et al.* Extensive genetics of ALS. Neurology 2012; 79(19): 1983.

Chiò A, Mazzini L, Alfonso S, Corrado L, Canosa A, Moglia C*, et al.* The multistep hypothesis of ALS revisited. Neurology 2018; 91(7): e635.

Choi SY, Lopez-Gonzalez R, Krishnan G, Phillips HL, Li AN, Seeley WW, *et al.* C9ORF72-ALS/FTD-associated poly(GR) binds Atp5a1 and compromises mitochondrial function in vivo. Nat Neurosci 2019; 22(6): 851-62.

Christensen JD, Kaufman MJ, Levin JM, Mendelson JH, Holman BL, Cohen BM, *et al.* Abnormal cerebral metabolism in polydrug abusers during early withdrawal: A 31P MR spectroscopy study. Magnetic Resonance in Medicine 1996; 35(5): 658-63.

Cichocka M, Kozub J, Urbanik A. PH Measurements of the Brain Using Phosphorus Magnetic Resonance Spectroscopy ((31)PMRS) in Healthy Men - Comparison of Two Analysis Methods. Pol J Radiol 2015; 80: 509-14.

Crugnola V, Lamperti C, Lucchini V, Ronchi D, Peverelli L, Prelle A, *et al.* Mitochondrial respiratory chain dysfunction in muscle from patients with amyotrophic lateral sclerosis. Archives of Neurology 2010; 67(7): 849-54.

Damiano M, Starkov AA, Petri S, Kipiani K, Kiaei M, Mattiazzi M, *et al.* Neural mitochondrial Ca2+ capacity impairment precedes the onset of motor symptoms in G93A Cu/Zn-superoxide dismutase mutant mice. Journal of neurochemistry 2006; 96(5): 1349-61.

de Albuquerque M, Branco LM, Rezende TJ, de Andrade HM, Nucci A, Franca MC, Jr. Longitudinal evaluation of cerebral and spinal cord damage in Amyotrophic Lateral Sclerosis. Neuroimage Clin 2017; 14: 269-76.

de Graaf RA. Spectral Quantification. In Vivo NMR Spectroscopy: John Wiley & Sons, Ltd; 2007. p. 445-77.

De Marco M, Merico A, Berta G, Segato N, Citton V, Baglione A, *et al.* Morphometric correlates of dysarthric deficit in amyotrophic lateral sclerosis. Amyotroph Lateral Scler Frontotemporal Degener 2015; 16(7-8): 464-72.

De Vos KJ, Hafezparast M. Neurobiology of axonal transport defects in motor neuron diseases: Opportunities for translational research? Neurobiology of Disease 2017; 105: 283-99.

De Vos KJ, Morotz GM, Stoica R, Tudor EL, Lau KF, Ackerley S, *et al.* VAPB interacts with the mitochondrial protein PTPIP51 to regulate calcium homeostasis. Hum Mol Genet 2012; 21(6): 1299-311.

DeJesus-Hernandez M, Mackenzie IR, Boeve BF, Boxer AL, Baker M, Rutherford NJ, *et al.* Expanded GGGGCC hexanucleotide repeat in noncoding region of C9ORF72 causes chromosome 9p-linked FTD and ALS. Neuron 2011; 72(2): 245-56.

Deng J, Wang P, Chen X, Cheng H, Liu J, Fushimi K, *et al.* FUS interacts with ATP synthase beta subunit and induces mitochondrial unfolded protein response in cellular and animal models. Proc Natl Acad Sci U S A 2018; 115(41): E9678-e86.

Desport JC, Preux PM, Magy L, Boirie Y, Vallat JM, Beaufrere B*, et al.* Factors correlated with hypermetabolism in patients with amyotrophic lateral sclerosis. Am J Clin Nutr 2001; 74(3): 328-34.

Desport JC, Torny F, Lacoste M, Preux PM, Couratier P. Hypermetabolism in ALS: correlations with clinical and paraclinical parameters. Neurodegener Dis 2005; 2(3-4): 202-7.

Dinh T, Doupis J, Lyons TE, Kuchibhotla S, Julliard W, Gnardellis C*, et al.* Foot muscle energy reserves in diabetic patients without and with clinical peripheral neuropathy. Diabetes care 2009; 32(8): 1521-4.

Dobrowolny G, Lepore E, Martini M, Barberi L, Nunn A, Scicchitano BM*, et al.* Metabolic Changes Associated With Muscle Expression of SOD1(G93A). Frontiers in physiology 2018; 9: 831-.

Dupuis L, di Scala F, Rene F, de Tapia M, Oudart H, Pradat PF*, et al.* Up-regulation of mitochondrial uncoupling protein 3 reveals an early muscular metabolic defect in amyotrophic lateral sclerosis. FASEB journal : official publication of the Federation of American Societies for Experimental Biology 2003; 17(14): 2091-3.

Dupuis L, Gonzalez de Aguilar JL, Echaniz-Laguna A, Eschbach J, Rene F, Oudart H*, et al.* Muscle mitochondrial uncoupling dismantles neuromuscular junction and triggers distal degeneration of motor neurons. PloS one 2009; 4(4): e5390.

Dupuis L, Pradat PF, Ludolph AC, Loeffler JP. Energy metabolism in amyotrophic lateral sclerosis. The Lancet Neurology 2011; 10(1): 75-82.

Echaniz-Laguna A, Zoll J, Ponsot E, N'Guessan B, Tranchant C, Loeffler JP*, et al.* Muscular mitochondrial function in amyotrophic lateral sclerosis is progressively altered as the disease develops: a temporal study in man. Experimental Neurology 2006; 198(1): 25-30.

Eleff SM, Barker PB, Blackband SJ, Chatham JC, Lutz NW, Johns DR*, et al.* Phosphorus magnetic resonance spectroscopy of patients with mitochondrial cytopathies demonstrates decreased levels of brain phosphocreatine. Annals of Neurology 1990; 27(6): 626-30.

Ellis CM, Suckling J, Amaro E, Jr., Bullmore ET, Simmons A, Williams SC*, et al.* Volumetric analysis reveals corticospinal tract degeneration and extramotor involvement in ALS. Neurology 2001; 57(9): 1571-8.

Ferreira GC, Pedersen PL. Phosphate transport in mitochondria: past accomplishments, present problems, and future challenges. Journal of Bioenergetics and Biomembranes 1993; 25(5): 483-92.

Ferri A, Coccurello R. What is "Hyper" in the ALS Hypermetabolism? Mediators of inflammation 2017; 2017: 7821672-.

Fujita K, Yamauchi M, Shibayama K, Ando M, Honda M, Nagata Y. Decreased cytochrome c oxidase activity but unchanged superoxide dismutase and glutathione peroxidase activities in the spinal cords of patients with amyotrophic lateral sclerosis. Journal of Neuroscience Research 1996; 45(3): 276-81.

Funalot B, Desport JC, Sturtz F, Camu W, Couratier P. High metabolic level in patients with familial amyotrophic lateral sclerosis. Amyotroph Lateral Scler 2009; 10(2): 113-7.

Gao J, Wang L, Yan T, Perry G, Wang X. TDP-43 proteinopathy and mitochondrial abnormalities in neurodegeneration. Mol Cell Neurosci 2019; 100: 103396.

Genin EC, Plutino M, Bannwarth S, Villa E, Cisneros-Barroso E, Roy M*, et al.* CHCHD10 mutations promote loss of mitochondrial cristae junctions with impaired mitochondrial genome maintenance and inhibition of apoptosis. EMBO Mol Med 2016; 8(1): 58-72.

Gorges M, Vercruysse P, Muller HP, Huppertz HJ, Rosenbohm A, Nagel G*, et al.* Hypothalamic atrophy is related to body mass index and age at onset in amyotrophic lateral sclerosis. J Neurol Neurosurg Psychiatry 2017; 88(12): 1033-41.

Gramegna LL, Giannoccaro MP, Manners DN, Testa C, Zanigni S, Evangelisti S*, et al.* Mitochondrial dysfunction in myotonic dystrophy type 1. Neuromuscul Disord 2018; 28(2): 144-9.

Grehl T, Fischer S, Muller K, Malin JP, Zange J. A prospective study to evaluate the impact of 31P-MRS to determinate mitochondrial dysfunction in skeletal muscle of ALS patients. Amyotrophic lateral sclerosis : official publication of the World Federation of Neurology Research Group on Motor Neuron Diseases 2007; 8(1): 4-8.

Hall CE, Yao Z, Choi M, Tyzack GE, Serio A, Luisier R*, et al.* Progressive Motor Neuron Pathology and the Role of Astrocytes in a Human Stem Cell Model of VCP-Related ALS. Cell Rep 2017; 19(9): 1739-49.

Hamakawa H, Murashita JUN, Yamada N, Inubushi T, Kato N, Kato T. Reduced intracellular pH in the basal ganglia and whole brain measured by 31P-MRS in bipolar disorder. Psychiatry and Clinical Neurosciences 2004; 58(1): 82-8.

Harwood CA, Westgate K, Gunstone S, Brage S, Wareham NJ, McDermott CJ*, et al.* Long-term physical activity: an exogenous risk factor for sporadic amyotrophic lateral sclerosis? Amyotrophic Lateral Sclerosis and Frontotemporal Degeneration 2016; 17(5-6): 377-84.

Hattingen E, Magerkurth J, Pilatus U, Mozer A, Seifried C, Steinmetz H*, et al.* Phosphorus and proton magnetic resonance spectroscopy demonstrates mitochondrial dysfunction in early and advanced Parkinson's disease. Brain 2009; 132(Pt 12): 3285-97.

Hoang TQ, Bluml S, Dubowitz DJ, Moats R, Kopyov O, Jacques D*, et al.* Quantitative proton-decoupled 31P MRS and 1H MRS in the evaluation of Huntington's and Parkinson's diseases. Neurology 1998; 50(4): 1033-40.

Hooijmans MT, Doorenweerd N, Baligand C, Verschuuren JJGM, Ronen I, Niks EH*, et al.* Spatially localized phosphorous metabolism of skeletal muscle in Duchenne muscular dystrophy patients: 24–month follow-up. PLOS ONE 2017a; 12(8): e0182086.

Hooijmans MT, Niks EH, Burakiewicz J, Verschuuren JJGM, Webb AG, Kan HE. Elevated phosphodiester and T(2) levels can be measured in the absence of fat infiltration in Duchenne muscular dystrophy patients. NMR in Biomedicine 2017b; 30(1): 10.1002/nbm.3667.

Hu MTM, Taylor-Robinson SD, Chaudhuri KR, Bell JD, Labbé C, Cunningham VJ*, et al.* Cortical dysfunction in non-demented Parkinson's disease patients: A combined 31P-MRS and 18FDG-PET study. Brain 2000; 123(2): 340-52.

Iotti S, Frassineti C, Alderighi L, Sabatini A, Vacca A, Barbiroli B. In vivo assessment of free magnesium concentration in human brain by 31P MRS. A new calibration curve based on a mathematical algorithm. NMR in biomedicine 1996; 9(1): 24-32.

Iotti S, Frassineti C, Alderighi L, Sabatini A, Vacca A, Barbiroli B. In vivo 31P-MRS assessment of cytosolic [Mg2+] in the human skeletal muscle in different metabolic conditions. Magnetic Resonance Imaging 2000; 18(5): 607-14.

Iotti S, Frassineti C, Sabatini A, Vacca A, Barbiroli B. Quantitative mathematical expressions for accurate in vivo assessment of cytosolic [ADP] and ΔG of ATP hydrolysis in the human brain and skeletal muscle. Biochimica et Biophysica Acta (BBA) - Bioenergetics 2005; 1708(2): 164-77.

Iotti S, Malucelli E. In vivo assessment of Mg2+ in human brain and skeletal muscle by 31P-MRS. Magnes Res 2008; 21(3): 157-62.

Jellinger KA. Cerebrospinal Fluid in Clinical Practice. European Journal of Neurology 2009; 16(5): e109-e.

Jeneson JA, Westerhoff HV, Brown TR, Van Echteld CJ, Berger R. Quasi-linear relationship between Gibbs free energy of ATP hydrolysis and power output in human forearm muscle. American Journal of Physiology-Cell Physiology 1995; 268(6): C1474-C84.

Jenkins TM, Alix JJP, David C, Pearson E, Rao DG, Hoggard N*, et al.* Imaging muscle as a potential biomarker of denervation in motor neuron disease. Journal of neurology, neurosurgery, and psychiatry 2018; 89(3): 248-55.

Kalra S. Magnetic Resonance Spectroscopy in ALS. Frontiers in Neurology 2019; 10: 482.

Kato T, Inubushi T, Kato N. Prediction of lithium response by 31P-MRS in bipolar disorder. International Journal of Neuropsychopharmacology 2000; 3(1): 83-5.

Kato T, Shioiri T, Murashita J, Hamakawa H, Takahashi Y, Inubushi T, *et al.* Lateralized abnormality of high energy phosphate metabolism in the frontal lobes of patients with bipolar disorder detected by phase-encoded 31P-MRS. Psychological Medicine 1995; 25(3): 557-66.

Kemp GJ, Ahmad RE, Nicolay K, Prompers JJ. Quantification of skeletal muscle mitochondrial function by 31P magnetic resonance spectroscopy techniques: a quantitative review. Acta Physiologica 2015; 213(1): 107-44.

Kemp GJ, Meyerspeer M, Moser E. Absolute quantification of phosphorus metabolite concentrations in human muscle in vivo by 31P MRS: a quantitative review. NMR in biomedicine 2007; 20(6): 555-65.

Kent-Braun JA, Miller RG. Central fatigue during isometric exercise in amyotrophic lateral sclerosis. Muscle Nerve 2000; 23(6): 909-14.

Kirkinezos IG, Bacman SR, Hernandez D, Oca-Cossio J, Arias LJ, Perez-Pinzon MA, *et al.* Cytochrome c association with the inner mitochondrial membrane is impaired in the CNS of G93A-SOD1 mice. The Journal of Neuroscience : the official journal of the Society for Neuroscience 2005; 25(1): 164-72.

Klunk WE, Xu C-J, Panchalingam K, McClure RJ, Pettegrew JW. Analysis of magnetic resonance spectra by mole percent: Comparison to absolute units. Neurobiology of aging 1994; 15(1): 133-40.

Ko YH, Hong S, Pedersen PL. Chemical mechanism of ATP synthase. Magnesium plays a pivotal role in formation of the transition state where ATP is synthesized from ADP and inorganic phosphate. The Journal of Biological Chemistry 1999; 274(41): 28853-6.

Kowaltowski AJ, Vercesi AE. Mitochondrial damage induced by conditions of oxidative stress. Free Radical Biology and Medicine 1999; 26(3): 463-71.

Krasnianski A, Deschauer M, Neudecker S, Gellerich FN, Muller T, Schoser BG, *et al.* Mitochondrial changes in skeletal muscle in amyotrophic lateral sclerosis and other neurogenic atrophies. Brain : a journal of neurology 2005; 128(Pt 8): 1870-6.

Kwiatkowski TJ, Jr., Bosco DA, Leclerc AL, Tamrazian E, Vanderburg CR, Russ C, *et al.* Mutations in the FUS/TLS gene on chromosome 16 cause familial amyotrophic lateral sclerosis. Science 2009; 323(5918): 1205-8.

Lacorte E, Ferrigno L, Leoncini E, Corbo M, Boccia S, Vanacore N. Physical activity, and physical activity related to sports, leisure and occupational activity as risk factors for ALS: A systematic review. Neurosci Biobehav Rev 2016; 66: 61-79.

Lehmer C, Schludi MH, Ransom L, Greiling J, Junghanel M, Exner N, *et al.* A novel CHCHD10 mutation implicates a Mia40-dependent mitochondrial import deficit in ALS. EMBO Mol Med 2018; 10(6).

Lodi R, Montagna P, Iotti S, Zaniol P, Barboni P, Puddu P, *et al.* Brain and muscle energy metabolism studied in vivo by 31P-magnetic resonance spectroscopy in NARP syndrome. J Neurol Neurosurg Psychiatry 1994; 57(12): 1492-6.

Ludtmann MHR, Arber C, Bartolome F, de Vicente M, Preza E, Carro E, *et al.* Mutations in valosin-containing protein (VCP) decrease ADP/ATP translocation across the mitochondrial membrane and impair energy metabolism in human neurons. J Biol Chem 2017; 292(21): 8907-17.

Luo G, Yi J, Ma C, Xiao Y, Yi F, Yu T, *et al.* Defective mitochondrial dynamics is an early event in skeletal muscle of an amyotrophic lateral sclerosis mouse model. PloS one 2013; 8(12): e82112-e.

Mahoney DJ, Kaczor JJ, Bourgeois J, Yasuda N, Tarnopolsky MA. Oxidative stress and antioxidant enzyme upregulation in SOD1-G93A mouse skeletal muscle. Muscle & Nerve 2006; 33(6): 809-16.

Mattiazzi M, D'Aurelio M, Gajewski CD, Martushova K, Kiaei M, Beal MF, *et al.* Mutated human SOD1 causes dysfunction of oxidative phosphorylation in mitochondria of transgenic mice. The Journal of Biological Chemistry 2002; 277(33): 29626-33.

Meyerspeer M, Boesch C, Cameron D, Dezortová M, Forbes SC, Heerschap A, *et al.* (31) P magnetic resonance spectroscopy in skeletal muscle: Experts' consensus recommendations. NMR in Biomedicine 2020: e4246-e.

Meyerspeer M, Kršśák M, Moser E. Relaxation times of 31P-metabolites in human calf muscle at 3 T. Magnetic Resonance in Medicine 2003; 49(4): 620-5.

Mierisová Š, Ala-Korpela M. MR spectroscopy quantitation: a review of frequency domain methods. NMR in Biomedicine 2001; 14(4): 247-59.

Morotz GM, De Vos KJ, Vagnoni A, Ackerley S, Shaw CE, Miller CC. Amyotrophic lateral sclerosis-associated mutant VAPBP56S perturbs calcium homeostasis to disrupt axonal transport of mitochondria. Hum Mol Genet 2012; 21(9): 1979-88.

Murphy E. Mysteries of Magnesium Homeostasis. Circulation Research 2000; 86(3): 245-8.

Nakaya T, Maragkakis M. Amyotrophic Lateral Sclerosis associated FUS mutation shortens mitochondria and induces neurotoxicity. Sci Rep 2018; 8(1): 15575.

Nalbandian A, Llewellyn KJ, Gomez A, Walker N, Su H, Dunnigan A*, et al.* In vitro studies in VCP-associated multisystem proteinopathy suggest altered mitochondrial bioenergetics. Mitochondrion 2015; 22: 1-8.

Naressi A, Couturier C, Devos JM, Janssen M, Mangeat C, Beer Rd*, et al.* Java-based graphical user interface for the MRUI quantitation package. Magnetic Resonance Materials in Physics, Biology and Medicine 2001; 12(2): 141.

Neumann M, Sampathu DM, Kwong LK, Truax AC, Micsenyi MC, Chou TT*, et al.* Ubiquitinated TDP-43 in frontotemporal lobar degeneration and amyotrophic lateral sclerosis. Science 2006; 314(5796): 130-3.

Neuwirth C, Nandedkar S, StåLberg E, Weber M. Motor unit number index (MUNIX): A novel neurophysiological technique to follow disease progression in amyotrophic lateral sclerosis. Muscle & Nerve 2010; 42(3): 379-84.

Nicholls DG. Bioenergetics. Fourth edition. ed: Amsterdam : Academic Press, 2013; 2013.

Onesto E, Colombrita C, Gumina V, Borghi MO, Dusi S, Doretti A*, et al.* Gene-specific mitochondria dysfunctions in human TARDBP and C9ORF72 fibroblasts. Acta Neuropathol Commun 2016; 4(1): 47.

Ordidge RJ, Bowley RM, McHale G. A general approach to selection of multiple cubic volume elements using the ISIS technique. Magnetic Resonance in Medicine 1988; 8(3): 323-31.

Ordidge RJ, Connelly A, Lohman JAB. Image-selected in Vivo spectroscopy (ISIS). A new technique for spatially selective nmr spectroscopy. Journal of Magnetic Resonance (1969) 1986; 66(2): 283-94.

Patel TB, Clark JB. Synthesis of N-acetyl-L-aspartate by rat brain mitochondria and its involvement in mitochondrial/cytosolic carbon transport. Biochem J 1979; 184(3): 539-46.

Peeters TH, van Uden MJ, Rijpma A, Scheenen TWJ, Heerschap A. 3D 31P MR spectroscopic imaging of the human brain at 3 T with a 31P receive array: An assessment of 1H decoupling, T1 relaxation times, 1H-31P nuclear Overhauser effects and NAD+. NMR in Biomedicine 2019; n/a(n/a): e4169.

Petersen KF, Dufour S, Shulman GI. Decreased insulin-stimulated ATP synthesis and phosphate transport in muscle of insulin-resistant offspring of type 2 diabetic parents. PLoS Medicine 2005; 2(9): e233-e.

Pioro EP. MR spectroscopy in amyotrophic lateral sclerosis/motor neuron disease. Journal of the neurological sciences 1997; 152 Suppl 1: S49-53.

Pioro EP, Majors AW, Mitsumoto H, Nelson DR, Ng TC. 1H-MRS evidence of neurodegeneration and excess glutamate + glutamine in ALS medulla. Neurology 1999; 53(1): 71-9.

Quadrelli S, Mountford C, Ramadan S. Hitchhiker's Guide to Voxel Segmentation for Partial Volume Correction of In Vivo Magnetic Resonance Spectroscopy. Magnetic Resonance Insights 2016; 9: 1-8.

Rata M, Giles SL, deSouza NM, Leach MO, Payne GS. Comparison of three reference methods for the measurement of intracellular pH using 31P MRS in healthy volunteers and patients with lymphoma. NMR in biomedicine 2014; 27(2): 158-62.

Ratai E-M, Alshikho MJ, Zürcher NR, Loggia ML, Cebulla CL, Cernasov P*, et al.* Integrated imaging of [11C]-PBR28 PET, MR diffusion and magnetic resonance spectroscopy 1H-MRS in amyotrophic lateral sclerosis. NeuroImage: Clinical 2018; 20: 357-64.

Redmond OM, Stack JP, O'Connor NG, Carney DN, Dervan PA, Hurson BJ*, et al.* 31P MRS as an early prognostic indicator of patient response to chemotherapy. Magnetic Resonance in Medicine 1992; 25(1): 30-44.

Renton AE, Majounie E, Waite A, Simon-Sanchez J, Rollinson S, Gibbs JR*, et al.* A hexanucleotide repeat expansion in C9ORF72 is the cause of chromosome 9p21-linked ALS-FTD. Neuron 2011; 72(2): 257-68.

Rijpma A, van der Graaf M, Meulenbroek O, Olde Rikkert MGM, Heerschap A. Altered brain high-energy phosphate metabolism in mild Alzheimer's disease: A 3-dimensional (31)P MR spectroscopic imaging study. NeuroImage Clinical 2018; 18: 254-61.

Rosen DR, Siddique T, Patterson D, Figlewicz DA, Sapp P, Hentati A*, et al.* Mutations in Cu/Zn superoxide dismutase gene are associated with familial amyotrophic lateral sclerosis. Nature 1993; 362(6415): 59-62.

Ryan TE, Erickson ML, Verma A, Chavez J, Rivner MH, McCully KK. Skeletal muscle oxidative capacity in amyotrophic lateral sclerosis. Muscle & nerve 2014; 50(5): 767-74.

Sharma KR, Kent-Braun JA, Majumdar S, Huang Y, Mynhier M, Weiner MW*, et al.* Physiology of fatigue in amyotrophic lateral sclerosis. Neurology 1995; 45(4): 733-40.

Shaw PJ. Molecular and cellular pathways of neurodegeneration in motor neurone disease. Journal of Neurology, Neurosurgery & Psychiatry 2005; 76(8): 1046.

Shimizu S, Kuriaki K. Effect of denervation on the total metal content of skeletal muscle. American Journal of Physiology-Legacy Content 1960; 198(5): 943-4.

Smith EF, Shaw PJ, De Vos KJ. The Role of Mitochondria in Amyotrophic Lateral Sclerosis. Neurosci Lett 2017; 710: 132933.

Song W, Song Y, Kincaid B, Bossy B, Bossy-Wetzel E. Mutant SOD1G93A triggers mitochondrial fragmentation in spinal cord motor neurons: Neuroprotection by SIRT3 and PGC-1α. Neurobiology of Disease 2013; 51: 72-81.

Soraru G, Vergani L, Fedrizzi L, D'Ascenzo C, Polo A, Bernazzi B*, et al.* Activities of mitochondrial complexes correlate with nNOS amount in muscle from ALS patients. Neuropathology and Applied Neurobiology 2007; 33(2): 204-11.

Sreedharan J, Blair IP, Tripathi VB, Hu X, Vance C, Rogelj B*, et al.* TDP-43 mutations in familial and sporadic amyotrophic lateral sclerosis. Science 2008; 319(5870): 1668-72.

Stefan D, Cesare FD, Andrasescu A, Popa E, Lazariev A, Vescovo E*, et al.* Quantitation of magnetic resonance spectroscopy signals: the jMRUI software package. Measurement Science and Technology 2009; 20(10): 104035.

Steyn FJ, Ioannides ZA, van Eijk RPA, Heggie S, Thorpe KA, Ceslis A*, et al.* Hypermetabolism in ALS is associated with greater functional decline and shorter survival. Journal of Neurology, Neurosurgery & Psychiatry 2018; 89(10): 1016.

Stoica R, Paillusson S, Gomez-Suaga P, Mitchell JC, Lau DH, Gray EH*, et al.* ALS/FTD-associated FUS activates GSK-3beta to disrupt the VAPB-PTPIP51 interaction and ER-mitochondria associations. EMBO Rep 2016; 17(9): 1326-42.

Straub IR, Janer A, Weraarpachai W, Zinman L, Robertson J, Rogaeva E*, et al.* Loss of CHCHD10-CHCHD2 complexes required for respiration underlies the pathogenicity of a CHCHD10 mutation in ALS. Hum Mol Genet 2018; 27(1): 178-89.

Tan W, Pasinelli P, Trotti D. Role of mitochondria in mutant SOD1 linked amyotrophic lateral sclerosis. Biochimica et Biophysica Acta (BBA) - Molecular Basis of Disease 2014; 1842(8): 1295-301.

Valkovič L, Chmelík M, Krššák M. In-vivo 31P-MRS of skeletal muscle and liver: A way for non-invasive assessment of their metabolism. Analytical Biochemistry 2017; 529: 193-215.

Vance JE. Phospholipid Synthesis and Transport in Mammalian Cells. Traffic 2015; 16(1): 1-18.

Vandoorne T, De Bock K, Van Den Bosch L. Energy metabolism in ALS: an underappreciated opportunity? Acta Neuropathologica 2018; 135(4): 489-509.

Vanhamme L, van den Boogaart A, Van Huffel S. Improved method for accurate and efficient quantification of MRS data with use of prior knowledge. Journal of Magnetic Resonance (San Diego, Calif : 1997) 1997; 129(1): 35-43.

Veech RL, Lawson JW, Cornell NW, Krebs HA. Cytosolic phosphorylation potential. J Biol Chem 1979; 254(14): 6538-47.

Vielhaber S, Winkler K, Kirches E, Kunz D, Buchner M, Feistner H, *et al.* Visualization of defective mitochondrial function in skeletal muscle fibers of patients with sporadic amyotrophic lateral sclerosis. Journal of the neurological sciences 1999; 169(1-2): 133-9.

Wang W, Wang L, Lu J, Siedlak SL, Fujioka H, Liang J, *et al.* The inhibition of TDP-43 mitochondrial localization blocks its neuronal toxicity. Nature medicine 2016; 22(8): 869-78.

Weiduschat N, Mao X, Beal MF, Nirenberg MJ, Shungu DC, Henchcliffe C. Usefulness of proton and phosphorus MR spectroscopic imaging for early diagnosis of Parkinson's disease. Journal of neuroimaging : official journal of the American Society of Neuroimaging 2015; 25(1): 105-10.

Wiedemann FR, Manfredi G, Mawrin C, Beal MF, Schon EA. Mitochondrial DNA and respiratory chain function in spinal cords of ALS patients. Journal of neurochemistry 2002; 80(4): 616-25.

Wiedemann FR, Winkler K, Kuznetsov AV, Bartels C, Vielhaber S, Feistner H, *et al.* Impairment of mitochondrial function in skeletal muscle of patients with amyotrophic lateral sclerosis. Journal of the Neurological Sciences 1998; 156(1): 65-72.

Wilson M, Andronesi O, Barker PB, Bartha R, Bizzi A, Bolan PJ, *et al.* Methodological consensus on clinical proton MRS of the brain: Review and recommendations. Magnetic Resonance in Medicine 2019; 82(2): 527-50.

Wu F, Jeneson JAL, Beard DA. Oxidative ATP synthesis in skeletal muscle is controlled by substrate feedback. American Journal of Physiology-Cell Physiology 2007; 292(1): C115-C24.

Zhou J, Yi J, Fu R, Liu E, Siddique T, Ríos E, *et al.* Hyperactive Intracellular Calcium Signaling Associated with Localized Mitochondrial Defects in Skeletal Muscle of an Animal Model of Amyotrophic Lateral Sclerosis. Journal of Biological Chemistry 2010; 285(1): 705-12.

Zochodne DW, Thompson RT, Driedger AA, Strong MJ, Gravelle D, Bolton CF. Metabolic changes in human muscle denervation: topical 31P NMR spectroscopy studies. Magnetic Resonance in Medicine 1988; 7(4): 373-83.

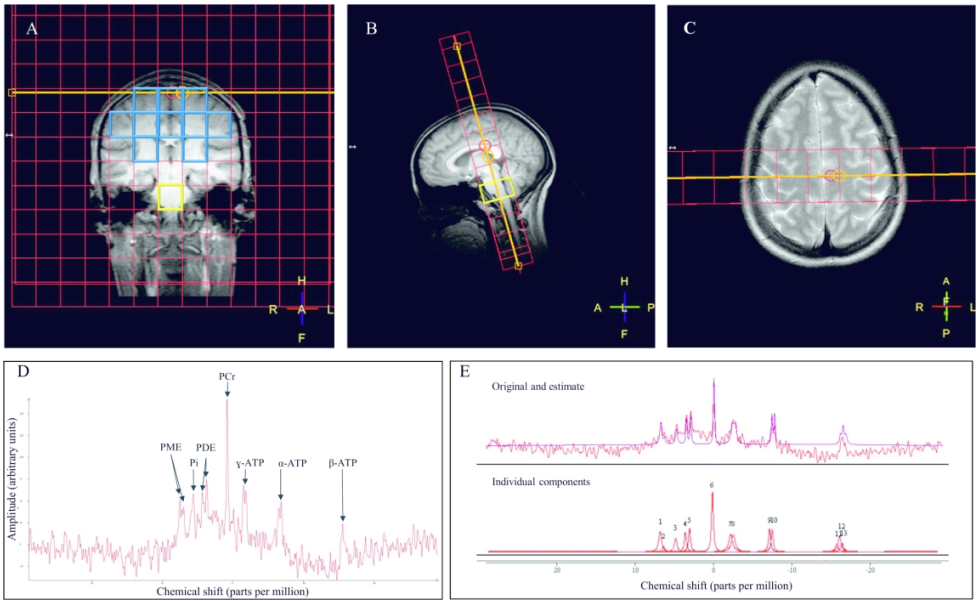

Figure 1 Anatomical localisation of the spectroscopic grid and example of fit of a brain spectrum acquired from the pons in a control.
Coronal (A), sagittal (B), and axial (C) images illustrate positioning of the spectroscopic grid encompassing motor cortex, descending corticospinal and corticobulbar tracts, and the pons. Voxels encompassing motor regions analysed in this study are depicted in blue and yellow in A. An example of a brain spectrum (D) acquired from the pons (voxel highlighted in yellow in A and B); resolved peaks are (from left to right): phosphomonoesters (PME – comprising phosphocholine and phosphoethanolamine peaks), inorganic phosphate (Pi), phosphodiesters (PDE - comprising glycerophosphoethanolamine and glycerophosphocholine), phosphocreatine (PCr), and the γ, α, and β phosphates of ATP. (E) illustrates spectral fitting: in the upper graph the estimated spectrum (in purple) is superimposed on to the raw data; in the graph below, individual resonances are depicted (1=phosphocholine; 2=phosphoethanolamine; 3=Pi; 4=glycerophosphoethanolamine; 5=glycerophosphocholine; 6=PCr; 7 and 8=γATP; 9 and 10=αATP; 11,12, and 13=βATP. Notably, γ and α ATP phosphates resonate as doublets and βATP as a triplet).

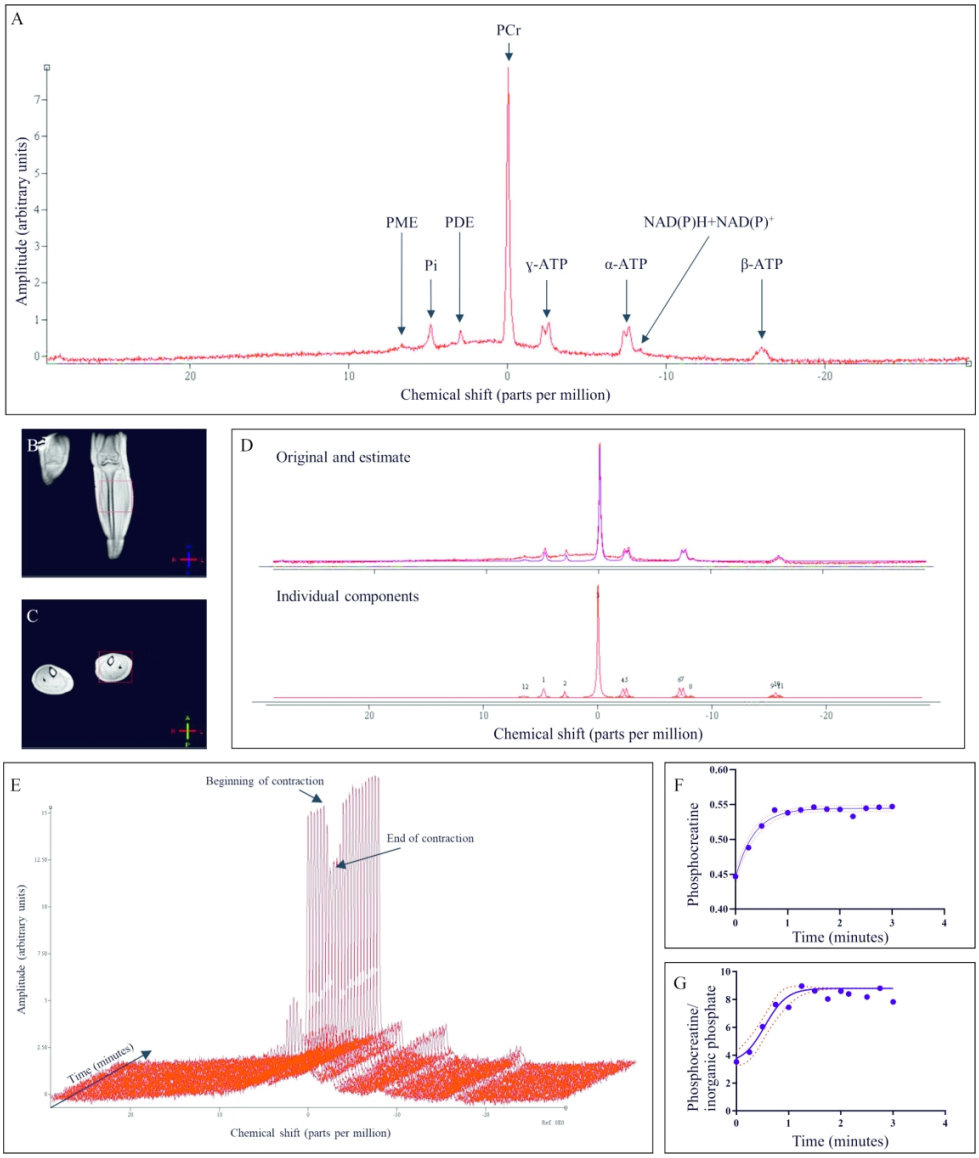

Figure 2 Anatomical localisation of muscle spectroscopy, example of fit of a muscle spectrum in a control, and dynamic muscle series.
In (A), a representative muscle spectrum acquired from a control's tibialis anterior at rest is illustrated. Resolved peaks are (from left to right): phosphomonoesters (PME), inorganic phosphate (Pi), phosphodiesters (PDE), phosphocreatine (PCr), γ and α resonances of adenosine triphosphate (ATP), nicotinamide adenine dinucleotides (NAD(P)+ and NAD(P)H), and β ATP. Localisation is depicted in B and C, the shimming box is depicted in red. (D) illustrates spectral fitting: in the upper graph the estimated spectrum (in purple) is superimposed on to the raw muscle data; in the graph below, individual resonances are depicted (1=Pi; 2=PDE; 3=PCr; 4 and 5=γATP; 6 and 7=αATP; 8= NAD(P)+ and NAD(P)H; 9, 10, and 11=βATP; 12=PME. Notably, γ and α ATP phosphates resonate as doublets and βATP as a triplet). (E) illustrates a dynamic time series: phosphocreatine drops substantially upon muscle contraction and gradually recovers to baseline values on cessation of exercise. Representative fitting of phosphocreatine/total phosphorus signal (F) and phosphocreatine/inorganic phosphate ratio (G) recovery values following cessation of exercise, the red lines represent error bars.

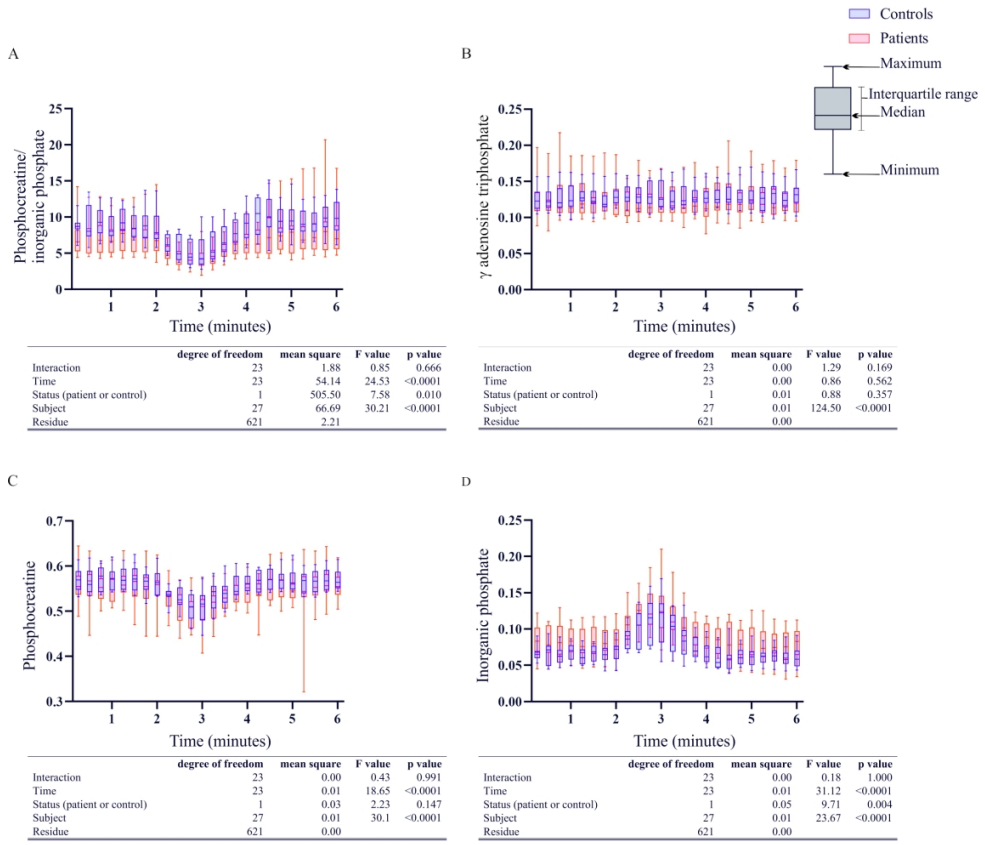

A	degree of freedom	mean square	F value	p value
Interaction	23	1.88	0.85	0.666
Time	23	54.14	24.53	<0.0001
Status (patient or control)	1	505.50	7.58	0.010
Subject	27	66.69	30.21	<0.0001
Residue	621	2.21		

B	degree of freedom	mean square	F value	p value
Interaction	23	0.00	1.29	0.169
Time	23	0.00	0.86	0.562
Status (patient or control)	1	0.01	0.88	0.357
Subject	27	0.01	124.50	<0.0001
Residue	621	0.00		

C	degree of freedom	mean square	F value	p value
Interaction	23	0.00	0.43	0.991
Time	23	0.01	18.65	<0.0001
Status (patient or control)	1	0.03	2.23	0.147
Subject	27	0.01	30.1	<0.0001
Residue	621	0.00		

D	degree of freedom	mean square	F value	p value
Interaction	23	0.00	0.18	1.000
Time	23	0.01	31.12	<0.0001
Status (patient or control)	1	0.05	9.71	0.004
Subject	27	0.01	23.67	<0.0001
Residue	621	0.00		

Figure 3 Dynamic time series depicting changes in metabolites in tibialis anterior following submaximal muscle contraction in controls (blue) and patients (red). Contraction begins at minute two and ends at minute three. All experiments were conducted at third of maximal voluntary isometric contraction force. Two-way repeated measures ANOVA statistics are reported below each graph. (A) Phosphocreatine/inorganic phosphate dynamics in patients and controls. (B) γ-adenosine triphosphate dynamics in patients and controls. (C) Phosphocreatine dynamics in patients and controls. (D) Inorganic phosphate dynamics in patients and controls. γATP, phosphocreatine, and inorganic phosphate are expressed as a proportion of total phosphorus signal.

Table 1 Participants' characteristics at time of scan.

	Controls *mean (±standard deviation)*	***Patients*** *mean (±standard deviation)*	***Means' difference*** *Patients-controls (±SEM)*	***t, DF***	***95% confidence interval***	***p***
Number of participants	10	20	*NA*	*NA*	*NA*	*NA*
Age (years)	57.30 (±10.90)	62.45 (±12.36)	5.15 (±4.42)	1.17, 20.32	-4.06 to 14.36	*0.257*
Gender	5 F : 5 M	7 F : 13 M	*NA*	*NA*	*NA*	*0.429*
Weight (Kilograms)	72.40 (±14.27)	74.50 (±12.31)	2.10 (±5.28)	0.40, 15.90	-9.11 to 13.31	*0.696*
10-metre walk test (seconds)	**4.45 (±0.61)**	**8.73 (±3.73)**	**4.28 (±0.90)**	**4.75, 18.77**	**2.39 to 6.17**	***<< 0.001****
Positive history of diabetes mellitus or pre-diabetes	none	none	*NA*	*NA*	*NA*	*NA*
Disease duration (months)	NA	29.04 (±24.36)	*NA*	*NA*	*NA*	*NA*
Revised ALS functional rating scale	NA	36.95 (±5.22)	*NA*	*NA*	*NA*	*NA*
Slow vital capacity (% predicted)	NA	85.60 (±22.85)	*NA*	*NA*	*NA*	*NA*
Upper motor neuron score	NA	10.22 (±2.92)	*NA*	*NA*	*NA*	*NA*
On riluzole	NA	16	*NA*	*NA*	*NA*	*NA*
Maximal voluntary isometric contraction (Kilograms)	**13.15 (±2.21)**	**8.25 (±5.68)**	***NA***	***NA***	***NA***	***0.002#****
Compound muscle action potential (millivolts)	**4.84 (±0.86)**	**3.37 (±1.34)**	**-1.48 (±0.41)**	**3.60, 25.76**	**-2.32 to -0.63**	***0.001****
Motor unit number index	**109.70 (±23.98)**	**66.67 (±29.54)**	**-43.00 (±10.17)**	**4.23, 22.07**	**-64.09 to -21.91**	***<< 0.001****
Motor unit size index (microvolts)	**44.67 (±4.62)**	**51.96 (±8.98)**	***NA***	***NA***	***NA***	***0.014#****

A chi-squared test was employed to test for gender matching, Mann-Whitney U test was applied in comparisons indicated by the hash symbol, for all other between-group comparisons, unpaired two-tailed t-tests with Welch correction were conducted. Asterisks indicate p values that remained significant after multiple comparisons correction. DF=Welch corrected degrees of freedom, F=female, M=male, NA=not applicable, SEM=standard error of mean.

Table 2 Spectroscopic parameters measured in the pons.

	Controls *mean (±standard deviation)*	***Patients*** *mean (±standard deviation)*	***Means' difference*** *Patients-controls (±SEM)*	***t, DF***	***95% confidence interval***	***p***
ΔG_{ATP} (kilojoule/mole)	**-61.12 (±1.88)**	**-59.12 (±1.56)**	***2.00 (±0.75)***	***2.68, 14.53***	***0.40 to 3.59***	***0.018***
γATP	0.15 (±0.03)	0.16 (±0.04)	*0.01 (±0.01)*	*0.43, 24.44*	*-0.02 to 0.04*	*0.668*
Phosphocreatine	**0.25 (±0.02)**	**0.21 (±0.04)**	**-0.04 (±0.01)**	**3.42, 26.44**	**-0.07 to -0.02**	***0.002****
Adenosine diphosphate (micromolar)	**169.60 (±64.85)**	**265.50 (±132.80)**	***95.86 (±40.53)***	***2.37, 21.42***	***11.68 to 180.00***	***0.028***
Inorganic phosphate	0.08 (±0.04)	0.09 (±0.04)	*0.02 (±0.02)*	*1.06, 17.29*	*-0.02 to 0.05*	*0.303*
pH	7.14 (±0.11)	7.07 (±0.07)	*-0.07 (±0.04)*	*1.70, 13.29*	*-0.15 to 0.02*	*0.113*
Free magnesium (millimolar)	0.13 (±0.05)	0.14 (±0.06)	*0.01 (±0.02)*	*0.59, 17.89*	*-0.03 to 0.06*	*0.563*
Phosphomonoesters	0.20 (±0.05)	0.18 (±0.04)	*-0.02 (±0.02)*	*1.15, 13.81*	*-0.06 to 0.02*	*0.270*
Phosphodiesters	0.17 (±0.04)	0.19 (±0.05)	*0.02 (±0.02)*	*1.32, 21.97*	*-0.01 to 0.06*	*0.199*

Unpaired two-tailed t-tests with Welch correction were conducted in all cases. Asterisks indicate values that remained significant after multiple comparisons correction. DF=Welch corrected degrees of freedom, SEM=standard error of mean, ΔG_{ATP}=Gibbs free energy of ATP hydrolysis (negative sign indicates that ATP hydrolysis is exergonic, amount of energy released is indicated by absolute ΔG_{ATP} values). γATP, phosphocreatine, inorganic phosphate, phosphomonoesters, and phosphodiesters are expressed as a proportion of total phosphorus signal.

Table 3 Spectroscopic parameters measured in tibialis anterior at rest.

	Controls *mean (±standard deviation)*	***Patients*** *mean (±standard deviation)*	***Means' difference*** *Patients-controls (±SEM)*	***t, DF***	***95% confidence interval***	***p***
ΔG_{ATP} (kilojoule/mole)	**-63.56 (±1.02)**	**-62.33 (±1.77)**	**NA**	**NA**	**NA**	***0.028#****
γATP	0.12 (±0.02)	0.12 (±0.02)	NA	NA	NA	*0.214#*
Phosphocreatine	0.56 (±0.02)	0.55 (±0.04)	-0.02 (±0.01)	1.78, 26.71	-0.04 to 0.00	*0.087*
Adenosine diphosphate (micromolar)	19.97 (±7.80)	35.78 (±32.34)	NA	NA	NA	*0.061#*
Inorganic phosphate	**0.06 (±0.01)**	**0.08 (±0.02)**	**0.02 (±0.01)**	**3.49, 27.45**	**0.01 to 0.03**	***0.002****
pH	**6.93 (±0.02)**	**6.96 (±0.03)**	**0.03 (±0.01)**	**2.96, 26.12**	**0.01 to 0.05**	***0.007****

Free magnesium (millimolar)	**0.43 (±0.11)**	**0.34 (±0.12)**	**NA**	**NA**	**NA**	***0.011#****
Phosphomonoesters	**0.02 (±0.01)**	**0.03 (±0.01)**	**0.01 (±0.00)**	**3.52, 27.73**	**0.00 to 0.02**	***0.002****
Phosphodiesters	0.07 (±0.02)	0.06 (±0.02)	-0.01 (±0.01)	1.01, 19.01	-0.02 to 0.01	*0.327*
NAD(P)H+NAD(P)$^+$	0.01 (±0.00)	0.01 (±0.01)	0.00 (±0.00)	1.16, 20.50	-0.01 to 0.00	*0.260*

Mann-Whitney U test was applied in comparisons indicated by the hash symbol, for all other between-group comparisons unpaired two-tailed t-tests with Welch correction were conducted. Asterisks indicate values that remained significant after multiple comparisons correction. DF=Welch corrected degrees of freedom, NAD(P)H+NAD(P)$^+$=nicotinamide adenine dinucleotides, SEM=standard error of mean, ΔG_{ATP}=Gibbs free energy of ATP hydrolysis (negative sign indicates that ATP hydrolysis is exergonic, amount of energy released is indicated by absolute ΔG_{ATP} values). γATP, phosphocreatine, inorganic phosphate, phosphomonoesters, phosphodiesters, and NAD(P)H+NAD(P)$^+$ are expressed as a proportion of total phosphorus signal.

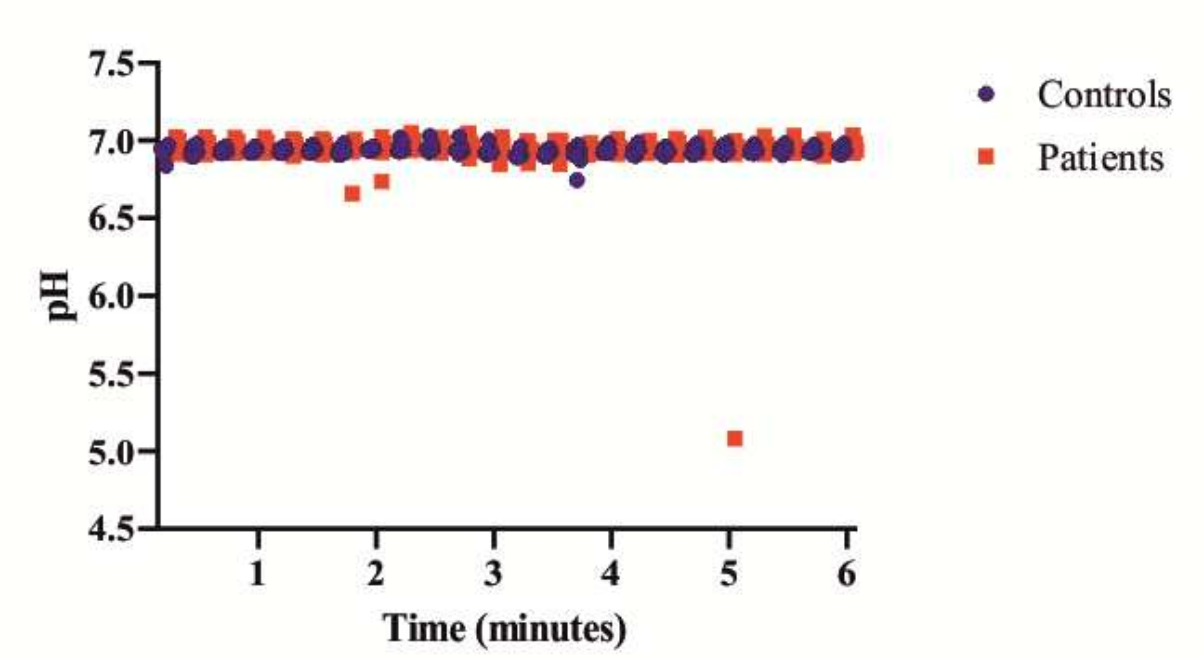

Supplementary figure 1 *pH dynamic time series of participants from whom phosphocreatine recovery constants were acquired. Data are acquired from tibialis anterior following submaximal muscle contraction in controls (blue) and patients (red); contraction begins at minute 2 and ends at minute 3. All experiments were conducted at third of maximal voluntary isometric contraction force.*

Abbreviations

ADP=adenosine diphosphate, ALS=amyotrophic lateral sclerosis, CI=95% confidence interval, ΔG_{ATP}=Gibbs free energy of ATP hydrolysis, ^{31}P-MRS=phosphorus-31 magnetic resonance spectroscopy.

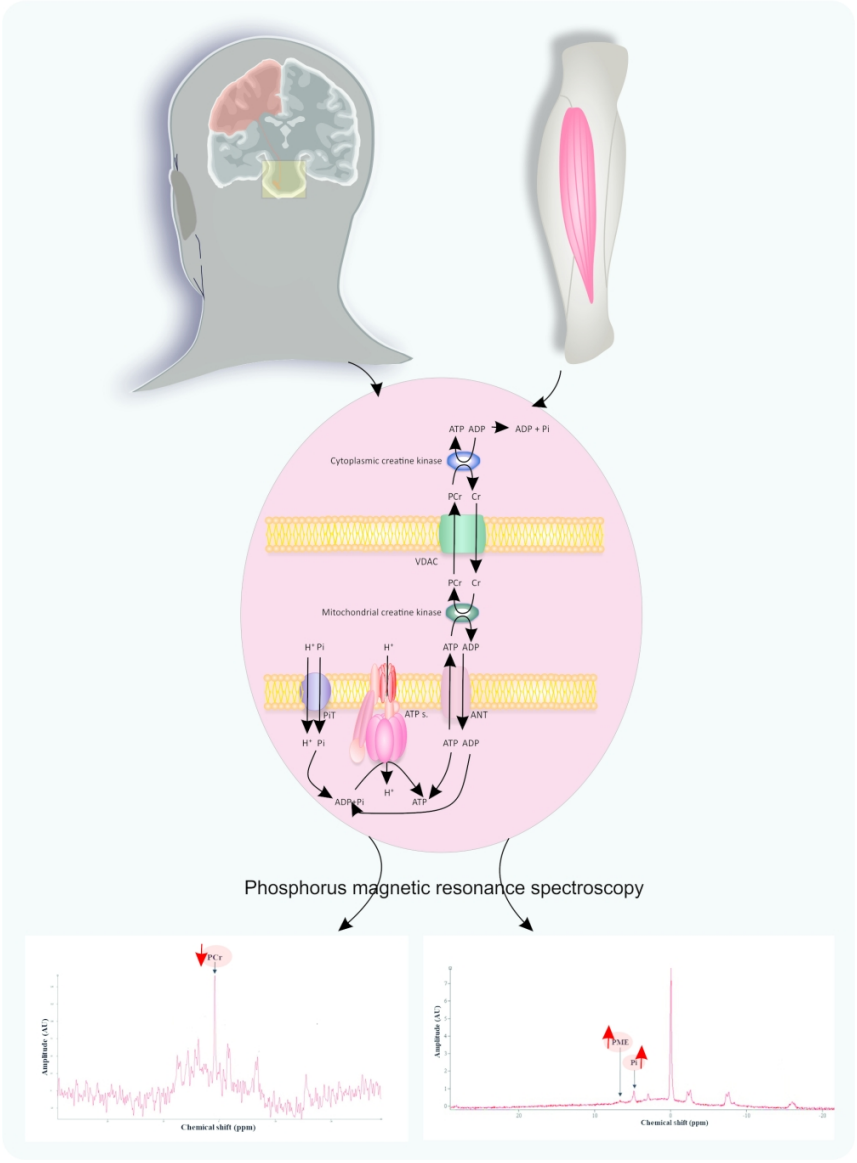

Phosphorus magnetic resonance spectroscopy reveals mitochondrial dysfunction in motor neuron disease

140x192mm (350 x 350 DPI)

STROBE statement: Reporting guidelines checklist for cohort, case-control and cross-sectional studies

SECTION	ITEM NUMBER	CHECKLIST ITEM	REPORTED ON PAGE NUMBER:
TITLE AND ABSTRACT			
	1a	Indicate the study's design with a commonly used term in the title or the abstract	2
	1b	Provide in the abstract an informative and balanced summary of what was done and what was found	2-3
INTRODUCTION			
Background and objectives	2	Explain the scientific background and rationale for the investigation being reported	4-7
	3	State specific objectives, including any pre-specified hypotheses	6-7
METHODS			
Study design	4	Present key elements of study design early in the paper	7
Setting	5	Describe the setting, locations, and relevant dates, including periods of recruitment, exposure, follow-up, and data collection	7
Participants	6a	Cohort study—Give the eligibility criteria, and the sources and methods of selection of participants. Describe methods of follow-up Case-control study—Give the eligibility criteria, and the sources and methods of case ascertainment and control selection. Give the rationale for the choice of cases and controls Cross-sectional study—Give the eligibility criteria, and the sources and methods of selection of participants	7-8
	6b	Cohort study—For matched studies, give matching criteria and number of exposed and unexposed Case-control study—For matched studies, give matching criteria and the number of controls per case Variables	7
Variables	7	Clearly define all outcomes, exposures, predictors, potential confounders, and effect modifiers. Give diagnostic criteria, if applicable	7-8, 11-14
Data sources/measurements	8*	For each variable of interest, give sources of data and details of methods of assessment	7-14

SECTION	ITEM NUMBER	CHECKLIST ITEM	REPORTED ON PAGE NUMBER:
		(measurement). Describe comparability of assessment methods if there is more than one group.	
Bias	9	Describe any efforts to address potential sources of bias.	9-14
Study size	10	Explain how the study size was arrived at	NA: first study of this type
Quantitative variables	11	Explain how quantitative variables were handled in the analyses. If applicable, describe which groupings were chosen and why.	11-14
Statistical methods	12a	Describe all statistical methods, including those used to control for confounding	12,14
	12b	Describe any methods used to examine subgroups and interactions	14
	12c	Explain how missing data were addressed	11-13
	12d	Cohort study—If applicable, explain how loss to follow-up was addressed Case-control study—If applicable, explain how matching of cases and controls was addressed Cross-sectional study—If applicable, describe analytical methods taking account of sampling strategy	7-8,13-14
	12e	Describe any sensitivity analyses	NA
RESULTS			
Participants	13a	Report numbers of individuals at each stage of study—eg numbers potentially eligible, examined for eligibility, confirmed eligible, included in the study, completing follow-up, and analysed	14
	13b	Give reasons for non-participation at each stage	14
	13c	Consider use of a flow diagram	NA
Descriptive Data	14a	Give characteristics of study participants (eg demographic, clinical, social) and information on exposures and potential confounders	14
	14b	Indicate number of participants with missing data for each variable of interest	14-17
	14c	Cohort study—Summarise follow-up time (eg, average and total amount)	NA
Outcome Data	15*	Cohort study—Report numbers of outcome events or summary measures over time Case-control study—Report numbers in each exposure category, or summary measures of exposure	14-17

SECTION	ITEM NUMBER	CHECKLIST ITEM	REPORTED ON PAGE NUMBER:
		Cross-sectional study—Report numbers of outcome events or summary measures	
Main Results	16a	Give unadjusted estimates and, if applicable, confounder-adjusted estimates and their precision (e.g. 95% confidence interval). Make clear which confounders were adjusted for and why they were included	14-15
	16b	Report category boundaries when continuous variables were categorized	Tables 1 to 3
	16c	If relevant, consider translating estimates of relative risk into absolute risk for a meaningful time period	NA
	16d	Report results of any adjustments for multiple comparisons	Tables 1 to 3
Other Analyses	17a	Report other analyses done—e.g. analyses of subgroups and interactions, and sensitivity analyses	14-17
	17b	If numerous genetic exposures (genetic variants) were examined, summarize results from all analyses undertaken	NA
	17c	If detailed results are available elsewhere, state how they can be accessed	17 →Suppl. materials
DISCUSSION			
Key Results	18	Summarise key results with reference to study objectives	17-24
Limitations	19	Discuss limitations of the study, taking into account sources of potential bias or imprecision. Discuss both direction and magnitude of any potential bias	23-24
Interpretation	20	Give a cautious overall interpretation of results considering objectives, limitations, multiplicity of analyses, results from similar studies, and other relevant evidence	17-24
Generalisability	21	Discuss the generalisability (external validity) of the study results Other information	17,24
FUNDING			
	22	Give the source of funding and the role of the funders for the present study and, if applicable, for the original study on which the present article is based	25

*Give information separately for cases and controls in case-control studies and, if applicable, for exposed and unexposed groups in cohort and cross-sectional studies.